PERGAMON

Deep-Sea Research I 47 (2000) 1621–1662

DEEP-SEA RESEARCH
PART I

Modeling phytoplankton blooms and carbon export production in the Southern Ocean: dominant controls by light and iron in the Atlantic sector in Austral spring 1992

C. Lancelot[a,*], E. Hannon[a], S. Becquevort[a], C. Veth[b], H.J.W. De Baar[b]

[a]*Ecologie des Systèmes Aquatiques, Université Libre de Bruxelles, CP221, Bd du Triomphe, B-1050, Belgium*
[b]*Netherlands Institute for Sea Research, P.O. Box 59, 1790 AB Den Burg, Texel, The Netherlands*

Received 10 September 1998; received in revised form 10 November 1999; accepted 10 November 1999

Abstract

The high nutrient low chlorophyll (HNLC) conditions of the Southern Ocean were explored with an ecological model (SWAMCO) describing the cycling of C, N, P, Si and Fe through different, aggregated, chemical and biological compartments of the plankton ecosystem. The structure of the model was chosen to take explicitly into account biological processes of importance in the formation and mineralization of carbon biomass in surface waters and in carbon export production. State variables include major inorganic nutrients (NO_3, NH_4, PO_4, $Si(OH)_4$), dissolved Fe, two groups of phytoplankton (diatoms and nanoflagellates), bacteria, heterotrophic nanoflagellates, microzooplankton, labile DOC and two classes of dissolved and particulate organic polymers with specific biodegradability. The model is closed by export production of particulate organic matter out of the surface layer and, when relevant, by metazooplanton, the grazing pressure of which is described as a forcing function. Parameterization was derived from the current knowledge on the kinetics of biological processes in the Southern Ocean and in other 'HNLC' areas. For its application in the Atlantic sector in spring 1992, the SWAMCO model was coupled 'off-line' to a 1D physical model forced by in situ meteorological and sea-ice conditions. The predictions of the model were successfully compared with chemical and biological observations recorded in the Antarctic circumpolar current (ACC) during the 1992 cruise ANTX/6 of RV *Polarstern*. In particular, the model simulates quite well the diatom bloom and carbon export event observed in the iron-enriched Polar Frontal region and the lack of ice-edge phytoplankton blooms in the marginal zone (MIZ) of the ACC area.

* Corresponding author. Fax: 322-650-59-93.
E-mail address: lancelot@ulb.ac.be (C. Lancelot).

0967-0637/00/$ - see front matter
PII: S0967-0637(00)00005-4

Model analysis shows that sufficient light and iron concentrations above 0.5 μmol m^{-3} are the necessary conditions for enhancing diatom blooms and particulate carbon export production in the Southern Ocean. Low iron availability prevents diatom growth but is still adequate for nanophytoplankton, the biomass of which is, however, kept to Chl a levels less than 1 mg m^{-3} due to the loss by the ubiquitous micrograzers. Little carbon export is predicted under iron-limitation conditions. Sensitivity tests conducted on the parameters describing iron and silicon uptake by diatoms reveal the complex nature of Fe and Si limitation in regulating the magnitude and extent of diatom blooms and carbon and opal export production in the Southern Ocean.

1. Introduction

The Southern Ocean is known to be a region with high nutrients but low chlorophyll (HNLC), and there is a need to understand this Antarctic Paradox. An understanding would allow to be addressed the role played by the Southern Ocean in global carbon cycling, hence its influence on global climate regulation. Within this region, the combined effects of wind stress and thermohaline circulation result in circumpolar divergence of surface waters and upwelling, which maintain high concentrations of all major nutrients in the surface layer (nitrate: 20–30 mmol m^{-3}; phosphate: 1.6–2 mmol m^{-3}; silicate: 30–100 mmol m^{-3} see e.g. Gordon et al., 1986). The light regime, highly seasonal, during summer reaches daily-integrated values as high as in the tropics (Campbell and Aarup, 1989). Despite the permanently high nutrient concentrations and seasonally high incident surface light, primary production is generally low (e.g. the review by Mathot et al., 1992). Mesoscale events of high productivity, however, do occur in (i) the Polar Front between 47° and 50°S (e.g. Bathmann et al., 1997); (ii) shallow, coastal embayments (e.g. Holm-Hansen and Mitchell, 1991); (iii) polynya (e.g. Arrigo et al., 1998a) and (iv) the vicinity of the retreating ice-edge (e.g. Smith and Nelson, 1985). Nevertheless, recorded maximum phytoplankton biomasses seldom reach the 25 mg Chl *a* m^{-3} expected from the nutrient stocks (Mitchell and Holm-Hansen, 1991).

Several hypotheses have been proposed to explain the paradox of high nutrients and low Chl a concentrations in the Southern Ocean. In a recent review, de Baar and Boyd (1999) suggest that phytoplankton growth in the Southern Ocean is under the triple control of (i) light availability driven by incident light, ice cover and wind stress; (ii) iron availability and (iii) micrograzing pressure. However, the degree to which physical, chemical and biological factors are co-limiting phytoplankton bloom events is not fully understood, and their relative importance may vary with location, time and local meteorological conditions (Lancelot et al., 1993).

The major role played by ice cover and the turbulence of the water column in controlling available light to phytoplankton, hence bloom initiation, has been shown by numerous field data. It is now admitted that deep-mixed ice-free areas are not highly productive and are dominated by nanoplankton communities (El-Sayed, 1984; Smetacek et al., 1990). On the other hand, many observations (e.g. Smith and Nelson,

1985, 1986; Nelson et al., 1987; Sullivan et al., 1988; Lancelot et al., 1991a, b) indicate that the circumpolar marginal ice zone is a region of enhanced primary production owing to the formation, at the time of ice melting, of a shallow vertically stable upper layer as a result of the production of melt water. Provided the ice-edge is well defined, these ice-edge related phytoplankton blooms trail the ice-edge as a narrow band 50–200 km wide (Smith and Nelson, 1985; Lancelot et al., 1993). Yet the phytoplankton biomass reached in these hydrodynamically stable areas, dominated by either nanophytoplankton (Hewes et al., 1990; Lancelot et al., 1993) or diatoms (Bianchi et al., 1993), remains modest (2–7 mg Chl a m^{-3}) considering the ambient nutrient concentrations. Furthermore, recent studies have showed that marginal ice zone phytoplankton blooms were absent at the receding ice-edge of the ACC in the Atlantic sector (Smetacek et al., 1997a,b) and in the Bellingshausen Sea (Turner and Owens, 1995).

Iron limitation of phytoplankton growth in this remote area, already suggested in 1931 (Gran, 1931), has been investigated since 1988 in several regions of the Southern Ocean in various Fe-enrichment experiments in shipboard microcosms: the Weddell and Scotia Sea (de Baar et al., 1990; Buma et al., 1991), the Drake Passage (Helbling et al., 1991), the Ross Sea (Martin et al., 1990) and the Atlantic sector of the Antarctic Circumpolar Current (van Leeuwe et al., 1997; Scharek et al., 1997). Bioassay results have shown that the addition of Fe consistently led to stimulation of the growth of the large diatoms. This impact of added Fe on large diatoms was also observed in other HNLC areas like the equatorial Pacific Ocean (Chavez et al., 1991; Fitzwater et al., 1996; Zettler et al., 1996) and the subarctic North Pacific Ocean (Boyd et al., 1996). More recently, the repeated intentional in situ iron enrichment experiment in the equatorial Pacific Ocean (Coale et al., 1996) also led to a diatom bloom (Cavenders-Bares et al., 1999). Apparently, diatom blooms depend on the availability of not only light and all three major nutrients N, P and Si but also some iron as suggested before (Harvey, 1933, 1937). From the modern evidence it can be concluded that the general low availability of dissolved Fe in HNLC areas is not limiting phytoplankton growth rate per se. Rather Fe availability is structuring the phytoplankton community, which in turn drives the structure of the dominant food web and export production (C-retaining microbial food-web versus C-exporting linear diatom to mesozooplankton food chain). The low Fe supply is indeed limiting the growth rate of large diatoms but is still sufficient for the development of pico- and nano-sized cells, better competitors at low nutrient concentration due to their larger surface : volume ratio (Morel et al., 1990). The biomass of these minute organisms is kept at a very low level by the grazing of the ubiquitous fast-growing protozoa (Frost and Franzen, 1992; Lancelot et al., 1993; Price et al., 1994). Recent bioassay studies on Antarctic diatoms (Takeda, 1998) show that iron limitation leads to more silicified, hence faster-sinking, diatoms, evidencing a more complex pattern of nutrient limitation interactions in HNLC ecosystems with consequences for the related biogeochemical cycles.

Considering the circumpolar variations in the distribution of dissolved iron (de Baar et al., 1999) and the large variability of meteorological conditions (in particular wind stress and sea ice prevailing at these high latitudes), the contribution of physical, chemical and biological factors to the control of phytoplankton bloom development is likely to greatly vary within the Southern Ocean, both geographically and temporally.

Phytoplankton experience forcing between two extremes — low trace metal concentration and windy meteorological conditions or sufficient trace metal concentration and serene meteorological conditions — giving rise to quite different phytoplankton species dominance and biomass, food-web structures and carbon export production.

Addressing the role of the Southern Ocean in global carbon cycling and its response to or influence on climate change requires the implementation of quite complex ecological models that incorporate the processes directing the structure of the planktonic system and their forcing functions. In particular, these models must explicitly describe trophic bifurcations, most notably the shift from the C-retaining microbial network towards the C-exporting linear food chain, under the triple control of light, nutrient availability and grazing pressure. Existing biological models of the Southern Ocean are generally limited to one phytoplankton and one zooplankton group (e.g. Goosse and Hecq, 1994) and include a maximum of 2 limiting nutrients — nitrate and silicic acid (e.g. Arrigo et al., 1998b). One exception is the biogeochemical model of Pondaven et al. (1998) developed for the simulation of the seasonal C, N and Si cycles at the ice-free Kerfix station located in the Indian Sector of the Southern Ocean. Their model structure includes 2 classes of phytoplankton and zooplankton and 3 nutrients (nitrate, ammonium, silicic acid). However, lacking iron as explicit nutrient it is not applicable for iron-limited areas. When we developed our simulation model there did not yet exist an ecosystem model incorporating iron as a limiting nutrient, either for the Southern Ocean or for any other oceanic region. Very recently, however, an iron-based ecosystem model has been reported for the central equatorial Pacific (Leonard et al., 1999), another HNLC area. Their model has nine components and includes nitrate, ammonium and iron as nutrient state variables. However, it does not explicitely consider the complex nature of nutrient-limitation interactions recently shown (Takeda, 1998; Hutchins and Bruland, 1998).

This paper presents the seawater microbial community (SWAMCO) model, a new version of the existing model of C and N cycling through the Antarctic microbial network (Lancelot et al., 1991a, b; 1993), upgraded with a view of extending its application at the scale of the whole Southern Ocean. In order to take into consideration the key role of iron in driving the structure and functioning of the Southern Ocean planktonic system and the related biogeochemical cycles, the structure of the biogeochemical model has been extended as follows: (i) all major nutrients (ammonium, nitrate, silicic acid and phosphate) and dissolved Fe are explicit state variables, allowing consideration of any nutrient limitation condition and any shift between limiting nutrients; (ii) two phytoplankton groups (nano-sized flagellates and large diatoms) are distinguished on the basis of their iron physiology, sinking rate and grazing control and (iii) the microbial network is explicitly described as composed of bacteria, autotrophic and bacterivorous nanoflagellates and microzooplankton, the last of which feed on both nanoflagellates (Becquevort, 1999). The parameterization procedure constitutes a key step for the successful implementation of an ecological model and the assessment of its prediction capability. The SWAMCO parameters were derived primarily from the available relevant data on Antarctic phytoplankton physiology and feeding activity of bacterivorous and herbivorous protozoa and, when such data did not exist, from the literature data on other HNLC areas.

The SWAMCO model was run in the Atlantic sector of the Southern Ocean covered by the ANT X/6 cruise of 1992 as a first assessment of the coherence of the model and of its capability to properly simulate phytoplankton bloom and carbon export events in the Southern Ocean under co-limitation of light and iron. This well-documented cruise was chosen because it had sampled repeatedly for 40 d along one section (6°W) crossing different water masses with contrasting ice coverage, hydrodynamical stability, iron concentration, diatom bloom and particulate export production (Smetacek et al., 1997a,b). The synergistic effects of light and iron in stimulating phytoplankton blooms and carbon export production in the Southern Ocean were further investigated with sensitivity tests of SWAMCO predictions to iron parameterization and iron-enrichment scenarios at contrasting latitudes of the ANT X/6 section. Finally, the recently reported interaction between iron limitation and diatom silicification and its consequence for opal export production was explored with sensitivity tests of SWAMCO predictions to the parameterization of diatom silicon uptake.

2. Model description

2.1. General structure of the swamco model

The structure of the SWAMCO model — state variables and processes linking them — is schematically illustrated in Fig. 1 and Table 1. It results from the assemblage of 3 sub-models reflecting the dynamics of the phytoplankton, the protozooplankton and the microbial loop. These model units, respectively, describe (i) the physiological growth of autotrophic nanoflagellates (NF) and diatoms (DA) according to the AQUAPHY conceptual model (Lancelot et al., 1991a); (ii) the bacterial degradation of both dissolved (D) and particulate (P) organic matter (for chemical elements C, N and P) according to the HSB model (Billen and Servais, 1988); (iii) the dynamics of herbivorous (microzooplankton MCZ) and bacterivorous (heterotrophic nanoflagelates HNF) protozoa (the HBP model, Becquevort, 1999). The uptake and regeneration fluxes of nitrate (NO_3), ammonia (NH_4), phosphate (PO_4) and dissolved iron (DFe) and silicon (DSi) are generated by the 3 sub-models, depicting the nutrient cycling.

The SWAMCO model is closed by mesozooplankton grazing pressure and export production out of the surface layer. The grazing by mesozooplankton on both diatoms and herbivorous protozoa is described as a forcing function, and no food preference is considered. Export production of key chemical elements C, N, Si and Fe into the deep ocean corresponds to the loss from the surface layer of particulate organic matter by sedimentation of both diatoms and dead (detrital) particulate matter (P), including fecal pellets. Due to their low density, the sedimentation of nanophytoplankton, bacteria and protozoa is neglected.

The differential equations describing the conservation of state variables are listed in Table 2. The kinetic expressions of the processes relative to the phytoplankton, protozooplankton and microbial loop modules are described in Table 3; process-related parameters are defined and listed in Table 4.

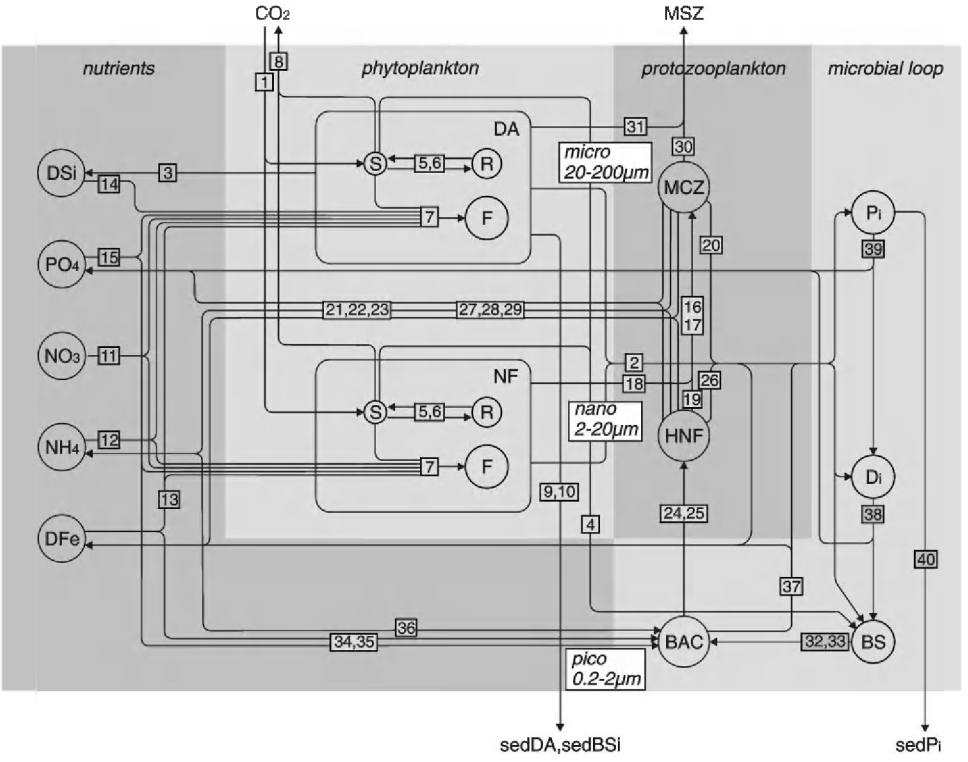

Fig. 1. Structure of the biogeochemical SWAMCO model (state variables and processes linking them are defined in Table 1).

2.2. Equations and parameterization

2.2.1. Phytoplankton dynamics

Each phytoplankton group (DA: diatoms; NF: nanoflagellates) is described by 3 state variables (functional cellular constituents F, reserve products R, monomeric substrates S) in order to distinguish between photosynthesis and growth processes (Lancelot et al., 1991a). Conceptually, this model is based on the notion of reserve product storage by phytoplankton cells, according to the future requirements of their growth. This was theoretically developed by Cohen and Parnas (1976) and experimentally demonstrated by Cuhel et al. (1984) and Lancelot et al. (1986). The photosynthetic process directly and the catabolism of storage products indirectly provide the energy and reductants required for the biosynthesis of new cellular material and for the maintenance of basal metabolism (Shuter, 1979). The production and loss processes are listed in Eqs. (V-1)–(V-6) (Table 2) and are described explicitly by Eqs. (P-1)–(P-15) (Table 3).

The rate of phytoplankton growth μ (Eq. (P-7), Table 3) is governed by the availability of intracellular monomers S and ambient inorganic nutrient N according

Table 1
SWAMCO model structure

Variable/Process	Symbol	Unit/meaning
(a) State variables		
Micro-organisms		
Diatoms		
Functional and structural metabolites	DAF	mmol C m^{-3}
Monomeric substrates	DAS	mmol C m^{-3}
Reserve material	DAR	mmol C m^{-3}
Biogenic Si	BSi	mmol Si m^{-3}
Autotrophic nanoflagellates		
Functional and structural metabolites	NFF	mmol C m^{-3}
Monomeric substrates	NFS	mmol C m^{-3}
Reserve material	NFR	mmol C m^{-3}
Microzooplankton	MCZ	mmol C m^{-3}
Heterotrophic nanoflagellates	HNF	mmol C m^{-3}
Bacteria	BAC	mmol C m^{-3}
Organic matter		
Monomeric substrates for bacteria	BSC	mmol C m^{-3}
	BSN	mmol N m^{-3}
Quickly biodegradable dissolved	DC1	mmol C m^{-3}
organic matter	DN1	mmol N m^{-3}
	DP1	mmol P m^{-3}
Quickly biodegradable particulate	PC1	mmol C m^{-3}
organic matter	PN1	mmol N m^{-3}
	PP1	mmol P m^{-3}
Slowly biodegradable dissolved	DC2	mmol C m^{-3}
organic matter	DN2	mmol N m^{-3}
	DP2	mmol P m^{-3}
Slowly biodegradable particulate	PC2	mmol C m^{-3}
organic matter	PN2	mmol N m^{-3}
	PP2	mmol P m^{-3}
Inorganic nutrients		
Nitrate	NO3	mmol N m^{-3}
Ammonium	NH4	mmol N m^{-3}
Phosphate	PO4	mmol P m^{-3}
Dissolved silica (silicic acid)	DSi	mmol Si m^{-3}
Dissolved iron	DFe	μmol Fe m^{-3}
(b) C and nutrients fluxes (see process equations in Table 3 and diagrammatic representation in Fig. 1)		
Phytoplankton dynamics		
1	φ_i	Photosynthesis ($i = 1$: diatoms; $i = 2$: nanoflagellates)
2	lys_j^i	Autolysis ($i = 1$: diatoms; $i = 2$: nanoflagellates) ($j = 1, 2, 3$ for F, S, R, see Table 1)
3	$\mathrm{lys}_{\mathrm{BSi}}$	Lysis of biogenic silica
4	e_i	Exudation ($i = 1$: diatoms; $i = 2$: nanoflagellates)

(*continued on next page*)

Table 1 (*continued*)

Variable/Process	Symbol	Unit/meaning
5	s_R^i	Synthesis of reserve products (R) ($i = 1$: diatoms; $i = 2$: nanoflagellates)
6	c_R^i	Catabolism of reserve products (R) ($i = 1$: diatoms; $i = 2$: nanoflagellates)
7	μ_i	Growth ($i = 1$: diatoms; $i = 2$: nanoflagellates)
8	$resp_i$	Respiration ($i = 1$: diatoms; $i = 2$: nanoflagellates)
9	sed_{DA}	Diatoms sedimentation
10	sed_{BSi}	Biogenic silica sedimentation
11	$upt_{PHY}^{NO_3}$	Nitrate uptake
12	$upt_{PHY}^{NH_4}$	Ammonium uptake
13	upt_{PHY}^{Fe}	Dissolved iron uptake
14	upt_{PHY}^{Si}	Silicic acid uptake
15	upt_{PHY}^{P}	Phosphate uptake
Protozooplankton dynamics		
Microzooplankton		
16	μ_{MCZ}	Growth
17	$graz_{MCZ}$	Grazing
18	$graz_{MC/NF}$	Grazing on autotrophic nanoflagellates
19	$graz_{MC/HNF}$	Grazing on heterotrophic nanoflagellates
20	lys_{MCZ}	Autolysis
21	reg_{MCZ}^{N}	Nitrogen regeneration
22	reg_{MCZ}^{P}	Phosphorus regeneration
23	reg_{MCZ}^{Fe}	Iron regeneration
Heterotrophic nanoflagellates		
24	μ_{HNF}	Growth
25	$graz_{HNF}$	Grazing
26	lys_{HNF}	Autolysis
27	reg_{HNF}^{N}	Nitrogen regeneration
28	reg_{HNF}^{P}	Phosphorus regeneration
29	reg_{HNF}^{Fe}	Iron regeneration
Mesozooplankton		
30	$graz_{MS/MC}$	Grazing on microzooplankton
31	$graz_{MS/DA}$	Grazing on diatoms
Microbial loop dynamics		
Bacteria		
32	μ_{BAC}	Growth
33	upt_{BAC}	Carbon uptake
34	upt_{BAC}^{P}	Phosphorus uptake
35	upt_{BAC}^{Fe}	Iron uptake
36	α_{BAC}	Ammonification
37	lys_{BAC}	Autolysis
Organic matter		
38	$elys_{D_i}$	Ecto-cellular hydrolysis of DC1, DN1, DP1, DC2, DN2, DP2
39	lys_{P_i}	Ecto-cellular hydrolysis of PC1, PN1, PP1, PC2, PN2, PP2
40	sed_{P_i}	Sedimentation of particulate organic matter

Table 2
SWAMCO model: conservation equations

Phytoplankton
DA: diatoms, NF: autotrophic nanoflagellates
F: functional + structural metabolites, S: monomeric substrates, R: reserve material

$$\mathrm{DA} = \mathrm{DAF} + \mathrm{DAS} + \mathrm{DAR}; \quad \mathrm{NF} = \mathrm{NFF} + \mathrm{NFS} + \mathrm{NFR}$$

$$\frac{\mathrm{dDAF}}{\mathrm{d}t} = \mu_{\mathrm{DA}} - \mathrm{lys}_{\mathrm{F}}^{\mathrm{DA}} - (\mathrm{graz}_{\mathrm{MS/DA}} + \mathrm{sed}_{\mathrm{DA}})\frac{\mathrm{DAF}}{\mathrm{DA}} \tag{V-1}$$

$$\frac{\mathrm{dDAS}}{\mathrm{d}t} = \varphi_{\mathrm{DA}} + c_{\mathrm{DAR}} - s_{\mathrm{DAR}} - \mu_{\mathrm{DA}} - \mathrm{resp}_{\mathrm{DA}} - \mathrm{lys}_{\mathrm{S}}^{\mathrm{DA}} - e_{\mathrm{DA}} - (\mathrm{graz}_{\mathrm{MS/DA}} + \mathrm{sed}_{\mathrm{DA}})\frac{\mathrm{DAS}}{\mathrm{DA}} \tag{V-2}$$

$$\frac{\mathrm{dDAR}}{\mathrm{d}t} = s_{\mathrm{DAR}} - c_{\mathrm{DAR}} - \mathrm{lys}_{\mathrm{R}}^{\mathrm{DA}} - (\mathrm{graz}_{\mathrm{MS/DA}} + \mathrm{sed}_{\mathrm{DA}})\frac{\mathrm{DAR}}{\mathrm{DA}} \tag{V-3}$$

$$\frac{\mathrm{dNFF}}{\mathrm{d}t} = \mu_{\mathrm{NF}} - \mathrm{lys}_{\mathrm{F}}^{\mathrm{NF}} - \mathrm{graz}_{\mathrm{MC/NF}}\frac{\mathrm{NFF}}{\mathrm{NF}} \tag{V-4}$$

$$\frac{\mathrm{dNFS}}{\mathrm{d}t} = \varphi_{\mathrm{NF}} + c_{\mathrm{NFR}} - s_{\mathrm{NFR}} - \mu_{\mathrm{NF}} - \mathrm{resp}_{\mathrm{NF}} - \mathrm{lys}_{\mathrm{S}}^{\mathrm{NF}} - e_{\mathrm{NF}} - \mathrm{graz}_{\mathrm{MC/NF}}\frac{\mathrm{NFS}}{\mathrm{NF}} \tag{V-5}$$

$$\frac{\mathrm{dNFR}}{\mathrm{d}t} = s_{\mathrm{NFR}} - c_{\mathrm{NFR}} - \mathrm{lys}_{\mathrm{R}}^{\mathrm{NF}} - \mathrm{graz}_{\mathrm{MC/NF}}\frac{\mathrm{NFR}}{\mathrm{NF}} \tag{V-6}$$

Protozooplankton
Micro-zooplankton (MCZ):

$$\frac{\mathrm{dMCZ}}{\mathrm{d}t} = \mu_{\mathrm{MCZ}} - \mathrm{lys}_{\mathrm{MCZ}} - \mathrm{graz}_{\mathrm{MS/MC}} \tag{V-7}$$

Heterotrophic nanoflagellates (HNF):

$$\frac{\mathrm{dHNF}}{\mathrm{d}t} = \mu_{\mathrm{HNF}} - \mathrm{lys}_{\mathrm{HNF}} - \mathrm{graz}_{\mathrm{MC/HNF}} \tag{V-8}$$

Bacteria (BAC), C and N monomeric substrates for bacteria (BSC, BSN)

$$\frac{\mathrm{dBAC}}{\mathrm{d}t} = \mu_{\mathrm{BAC}} - \mathrm{lys}_{\mathrm{BAC}} - \mathrm{graz}_{\mathrm{HNF}} \tag{V-9}$$

$$\frac{\mathrm{dBSC}}{\mathrm{d}t} = \mathrm{elys}_{\mathrm{D1}} + \mathrm{elys}_{\mathrm{D2}} + \mathrm{lys}_{\mathrm{S}}^{\mathrm{DA}} + \mathrm{lys}_{\mathrm{S}}^{\mathrm{NF}} + e_{\mathrm{DA}} + e_{\mathrm{NF}} - \mathrm{upt}_{\mathrm{BAC}} \tag{V-10}$$

$$\frac{\mathrm{dBSN}}{\mathrm{d}t} = \mathrm{elys}_{\mathrm{D}_1}\frac{\mathrm{DN}_1}{\mathrm{DC}_1} + \mathrm{elys}_{\mathrm{D}2}\frac{\mathrm{DN}_2}{\mathrm{DC}_2} - \mathrm{upt}_{\mathrm{BAC}}\frac{\mathrm{BSN}}{\mathrm{BSC}} \tag{V-11}$$

Organic matter (D = dissolved, P = particulate, i: 1. quickly, 2. slowly biodegradable substrates)

$$\frac{\mathrm{dDC}_i}{\mathrm{d}t} = \varepsilon_{\mathrm{d}}^{i}\mathrm{lys}_{\mathrm{bio}} + \mathrm{lys}_{\mathrm{PC}_i} - \mathrm{elys}_{\mathrm{D}_i} \tag{V-12}$$

$$\frac{\mathrm{dPC}_i}{\mathrm{d}t} = \varepsilon_{\mathrm{p}}^{i}\mathrm{lys}_{\mathrm{bio}} - \mathrm{lys}_{\mathrm{PC}_i} - \mathrm{sed}_{\mathrm{PC}_i} \tag{V-13}$$

(*continued on next page*)

Table 2 (*continued*)

with

$$\mathrm{lys_{bio}} = \mathrm{lys_F^{DA}} + \mathrm{lys_R^{DA}} + \mathrm{lys_F^{NF}} + \mathrm{lys_R^{NF}} + \mathrm{lys_{MCZ}} + \mathrm{lys_{HNF}} + \mathrm{lys_{BAC}}$$

$$\frac{\mathrm{dDN}_i}{\mathrm{d}t} = \varepsilon_{\mathrm{d}}^i \mathrm{lys}N_{\mathrm{bio}} + \mathrm{lys_{PN_i}} - \mathrm{elys_{DC_i}}\frac{\mathrm{DN}_i}{\mathrm{DC}_i} \tag{V-14}$$

$$\frac{\mathrm{dPN}_i}{\mathrm{d}t} = \varepsilon_{\mathrm{p}}^i \mathrm{lys}N_{\mathrm{bio}} - \mathrm{lys_{PN}}i - \mathrm{sed_{PN}}i \tag{V-15}$$

with

$$\mathrm{lys}N_{\mathrm{bio}} = \frac{\mathrm{lys_F^{DA}} + \mathrm{lys_F^{NF}}}{\mathrm{CN_{PHY}}} + \frac{\mathrm{lys_{MCZ}} + \mathrm{lys_{HNF}}}{\mathrm{CN_{ZOO}}} + \frac{\mathrm{lys_{BAC}}}{\mathrm{CN_{BAC}}}$$

$$\frac{\mathrm{dDP}_i}{\mathrm{d}t} = \varepsilon_{\mathrm{d}}^i \mathrm{lys}P_{\mathrm{bio}} - \mathrm{elys_{DC_i}}\frac{\mathrm{DP}_i}{\mathrm{DC}_i} \tag{V-16}$$

$$\frac{\mathrm{dPP}_i}{\mathrm{d}t} = \varepsilon_{\mathrm{p}}^i \mathrm{lys}P_{\mathrm{bio}} - \mathrm{lys_{PP_i}} - \mathrm{sed_{PP_i}} \tag{V-17}$$

$$\text{with} \quad \mathrm{lys}P_{\mathrm{bio}} = \frac{\mathrm{lys_F^{DA}} + \mathrm{lys_F^{NF}}}{\mathrm{CP_{PHY}}} + \frac{\mathrm{lys_{MCZ}} + \mathrm{lys_{HNF}}}{\mathrm{CP_{ZOO}}} + \frac{\mathrm{lys_{BAC}}}{\mathrm{CP_{BAC}}}$$

Nutrients

$$\frac{\mathrm{dNO_3}}{\mathrm{d}t} = -\mathrm{upt_{PHY}^{NO_3}} \tag{V-18}$$

$$\frac{\mathrm{dNH_4}}{\mathrm{d}t} = \alpha_{\mathrm{BAC}} + \mathrm{reg_{MCZ}^N} + \mathrm{reg_{HNF}^N} - \mathrm{upt_{PHY}^{NH_4}} \tag{V-19}$$

$$\frac{\mathrm{dPO_4}}{\mathrm{d}t} = \mathrm{elys_{D_1}}\frac{\mathrm{DP_1}}{\mathrm{DC_1}} + \mathrm{lys_{PP1}} + \mathrm{elys_{D2}}\frac{\mathrm{DP_2}}{\mathrm{DC_2}} + \mathrm{lys_{PP2}} + \mathrm{reg_{MCZ}^P} + \mathrm{reg_{HNF}^P} - \mathrm{upt_{PHY}^P} - \mathrm{upt_{BAC}^P} \tag{V-20}$$

$$\frac{\mathrm{dDSi}}{\mathrm{d}t} = \mathrm{lys_{BSi}} - \mathrm{upt_{DA}^{Si}} \tag{V-21}$$

$$\frac{\mathrm{dBSi}}{\mathrm{d}t} = \mathrm{upt_{DA}^{Si}} - \mathrm{lys_{BSi}} - \mathrm{sed_{BSi}} \tag{V-22}$$

$$\frac{\mathrm{dDFe}}{\mathrm{d}t} = \mathrm{reg_{MCZ}^{Fe}} + \mathrm{reg_{HNF}^{Fe}} + \mathrm{lys_{bio}^{Fe}} - \mathrm{upt_{PHY}^{Fe}} - \mathrm{upt_{BAC}^{Fe}} \tag{V-23}$$

$$\text{with} \quad \mathrm{lys_{bio}^{Fe}} = \mathrm{lys_F^{DA}FeC_{DA}} + \mathrm{lys_F^{NF}FeC_{NF}} + (\mathrm{lys_{MCZ}} + \mathrm{lys_{HNF}})\mathrm{FeC_{ZOO}} + \mathrm{lys_{BAC}FeC_{BAC}}$$

to a multiplicative Michaelis–Menten kinetics characterized by 3 constants: the maximum specific growth rate μmax and the half-saturation constants for the assimilation of S (k_S) and nutrient. One single nutrient is considered as limiting phytoplankton growth. It corresponds to the nutrient that displays the lowest ambient concentration compared to the half-saturation constant for phytoplankton uptake. Conceptually, it can be either inorganic N (NO_3 + NH4), Si, PO4 or Fe, and the

Table 3
SWAMCO model: kinetic expressions of the processes

Phytoplankton dynamics ($i = 1, 2$: diatoms DA, nanoflagellates NF)
Photosynthesis:

$$\varphi_i = k_{\max}(1 - e^{-\alpha I/k_{\max}})(e^{-\beta I/k_{\max}})\, F_i \quad \text{(P-1)}$$

with

$$I = I_0((1 - a_{\text{ice}})\text{ice} + (1 - a_{\text{sea}})(1 - \text{ice}))e^{-\eta z}, \quad a_{\text{ice}} = 0.95; \quad a_{\text{sea}} = 0.15$$

where I_0 is the incident PAR [μmole m^{-2} s^{-1}]; z the depth [m]; and ice the ice cover [fraction]

$$\eta = 0.042 + 0.025\chi \sum_{i:\text{DA,NF}} F_i$$

Lysis and exudation:

$$\text{lys}_F^i = k_{\text{lys}} F_i; \quad \text{lys}_S^i = k_{\text{lys}} S_i; \quad \text{lys}_R^i = k_{\text{lys}} R_i \quad \text{(P-2)}$$

$$\text{lys}_{\text{BSi}} = k_{\text{lys}}\text{BSi} \quad \text{(P-3)}$$

$$e_i = \varepsilon\varphi_i \quad \text{(P-4)}$$

Synthesis (s) and catabolism (c) of reserve products:

$$s_{\text{R}}^i = \rho_{\max}\frac{S^{\text{ut}}}{S^{\text{ut}} + k_{\text{s}}} F_i \quad \text{with } S^{\text{ut}} = S_i/F_i - Q_s \quad \text{(P-5)}$$

$$c_{\text{R}}^i = k_{\text{c}}^{\text{R}} R_i \quad \text{(P-6)}$$

Growth and respiration:

$$\mu_i = \mu_{\max}\frac{S^{\text{ut}}}{S^{\text{ut}} + k_{\text{s}}}\tilde{N}F_i \quad \text{(P-7)}$$

$$\text{with} \quad \tilde{N} = \min\left(\frac{N^{\text{ut}}}{N^{\text{ut}} + k_{\text{N}}}, \frac{P^{\text{ut}}}{P^{\text{ut}} + k_{\text{P}}}, \frac{Fe^{\text{ut}}}{Fe^{\text{ut}} + k_{\text{Fe}}^i}, \left[\frac{Si^{\text{ut}}}{Si^{\text{ut}} + k_{\text{Si}}}\right]^{(*)}\right)$$

$$N^{\text{ut}} = \text{NO}_3 + \text{NH}_4 - {}^{k_N/10}$$

$$P^{\text{ut}} = \text{PO}_4 - kp/10$$

$$Fe^{\text{ut}} = \text{DFe} - ki_{\text{e}}/10$$

$$\text{Si}^{\text{ut}} = \text{DSi} - kS_{\text{i}}/10 \quad (*) \text{ diatoms only}$$

$$\text{resp}_i = K_{\text{F}} F_i + \xi\mu_i \quad \text{(P-8)}$$

$$\text{with} \quad \xi = \text{ecs}_{\text{NH}_4}(1 - f_{\text{NO}_3}) + \text{ecs}_{\text{NO}_3} f_{\text{NO}_3} \quad \text{(metabolic cost)}$$

Sedimentation (diatoms, biogenic silica):

$$\text{sed}_{\text{DA}} = k_{\text{sed}}(\text{DAF} + \text{DAS} + \text{DAR}) \quad \text{(P-9)}$$

$$\text{sed}_{\text{BSi}} = k_{\text{sed}}\text{BSi} \quad \text{(P-10)}$$

$$\text{with} \quad k_{\text{sed}} = V_{\text{sed}}/\tfrac{1}{2}\text{WML}_{\text{depth}}$$

(*continued on next page*)

Table 3 (*continued*)

Nutrients uptake:

$$\mathrm{upt}^{\mathrm{NO_3}}_{\mathrm{PHY}} = \frac{f_{\mathrm{NO_3}}}{\mathrm{CN_{PHY}}} \sum_{i:\mathrm{DA,NF}} \mu_i \tag{P-11}$$

with $f_{\mathrm{NO_3}} = 1 - I_m \mathrm{NH_4}/(\mathrm{NH_4} + K_i)$

$$\mathrm{upt}^{\mathrm{NH_4}}_{\mathrm{PHY}} = \frac{1 - f_{\mathrm{NO_3}}}{\mathrm{CN_{PHY}}} \sum_{i:\mathrm{DA,NF}} \mu_i \tag{P-12}$$

$$\mathrm{upt}^{\mathrm{Fe}}_{\mathrm{PHY}} = \sum_{i:\mathrm{DA,NF}} (\mu_i \mathrm{FeC}_i) \tag{P-13}$$

$$\mathrm{upt}^{\mathrm{Si}}_{\mathrm{DA}} = \mu_{\mathrm{DA}} \mathrm{SiC} \tag{P-14}$$

with $\mathrm{SiC} = [\mathrm{Si}:\mathrm{C}]_0 + \Phi \mathrm{DFe}$

$$\mathrm{upt}^{P}_{\mathrm{PHY}} = \frac{1}{\mathrm{CP}} \sum_{i:\mathrm{DA,NF}} \mu_i \tag{P-15}$$

Protozooplankton dynamics
Microzooplankton
Grazing on nano-flagellates:

$$\mu_{\mathrm{MCZ}} = y_{\mathrm{ZOO}} \mathrm{graz}_{\mathrm{MCZ}} \tag{P-16}$$

$$\mathrm{graz}_{\mathrm{MCZ}} = \mathrm{graz}^{\mathrm{MCZ}}_{\mathrm{max}} \frac{f_{\mathrm{ut}}}{f_{\mathrm{ut}} + k^{\mathrm{mcz}}_g} \mathrm{MCZ} \tag{P-17}$$

with

$$f_{\mathrm{ut}} = (\mathrm{NFF} + \mathrm{NFS} + \mathrm{NFR}) + \mathrm{HNF} - \mathrm{ths}_{\mathrm{MCZ}}$$

$$\mathrm{graz}_{\mathrm{MC/NF}} = \mathrm{graz}_{\mathrm{MCZ}} \frac{\mathrm{NF}}{\mathrm{NF} + \mathrm{HNF}} \tag{P-18}$$

$$\mathrm{graz}_{\mathrm{MC/HNF}} = \mathrm{graz}_{\mathrm{MCZ}} \frac{\mathrm{HNF}}{\mathrm{NF} + \mathrm{HNF}} \tag{P-19}$$

Lysis:

$$\mathrm{lys}_{\mathrm{MCZ}} = k^{\mathrm{ZOO}}_{\mathrm{d}} \mathrm{MCZ} \tag{P-20}$$

Nutrient regeneration

$$\mathrm{reg}^{\mathrm{N}}_{\mathrm{MCZ}} = \mathrm{graz}_{\mathrm{MCZ}} \mathrm{NFF}/\mathrm{CN_{phy}} + \frac{\mathrm{HNF}/\mathrm{CN_{ZOO}}}{\mathrm{NF} + \mathrm{HNF}} - \mu_{\mathrm{MCZ}}/\mathrm{CN_{ZOO}} \tag{P-21}$$

$$\mathrm{reg}^{\mathrm{P}}_{\mathrm{MCZ}} = \mathrm{graz}_{\mathrm{MCZ}} \frac{\mathrm{NFF}/\mathrm{CP_{phy}} + \mathrm{HNF}/\mathrm{CP_{ZOO}}}{\mathrm{NF} + \mathrm{HNF}} - \mu_{\mathrm{MCZ}}/\mathrm{CP_{ZOO}} \tag{P-22}$$

$$\mathrm{reg}^{\mathrm{Fe}}_{\mathrm{MCZ}} = \mathrm{graz}_{\mathrm{MCZ}} \frac{\mathrm{NFF}\,\mathrm{FeC_{NF}} + \mathrm{HNFFeC_{ZOO}}}{\mathrm{NF} + \mathrm{HNF}} - \mu_{\mathrm{MCZ}} \mathrm{FeC_{ZOO}} \tag{P-23}$$

Table 3 (*continued*)

Heterotrophic nano-flagellates
Grazing on bacteria:

$$\mu_{HNF} = y_{ZOO}\,graz_{HNF} \tag{P-24}$$

$$graz_{HNF} = graz_{max}^{HNF}\frac{f_{ut}}{f_{ut} + k_g}HNF \tag{P-25}$$

with $f_{ut} = BAC - ths_{HNF}$

Lysis:

$$lys_{HNF} = k_d^{ZOO}HNF \tag{P-26}$$

Nutrient regeneration:

$$reg_{HNF}^{N} = \frac{graz_{HNF}}{CN_{BAC}} - \frac{\mu_{HNF}}{CN_{ZOO}} \tag{P-27}$$

$$reg_{HNF}^{P} = \frac{graz_{HNF}}{CP_{BAC}} - \frac{\mu_{HNF}}{CP_{ZOO}} \tag{P-28}$$

$$reg_{HNF}^{Fe} = graz_{HNF}FeC_{BAC} - \mu_{HNF}FeC_{ZOO} \tag{P-29}$$

Grazing by mesozooplankton on diatoms and microzooplankton

$$graz_{MS/MC} = graz_{MSZ}\frac{MCZ}{MCZ + DA} \tag{P-30}$$

$$graz_{MS/DA} = graz_{MSZ}\frac{DA}{MCZ + DA} \tag{P-31}$$

with $DA = DAF + DAS + DAR$ $graz_{MSZ}$: forcing function.

Microbial loop dynamics
Bacteria
Growth:

$$\mu_{BAC} = upt_{BAC}y_{BAC} \tag{P-32}$$

$$upt_{BAC} = b_{max}\frac{S^{ut}}{S^{ut} + k_{BSC}}BAC \tag{P-33}$$

with $S^{ut} = BSC - \frac{k_{BSC}}{10}$

P and Fe uptake:

$$upt_{BAC}^{P} = \frac{\mu_{BAC}}{CP_{BAC}} \tag{P-34}$$

$$upt_{BAC}^{Fe} = \mu_{BAC}FeC_{BAC} \tag{P-35}$$

Ammonification:

$$\alpha_{BAC} = upt_{BAC}\frac{BSN}{BSC} - \frac{\mu_{BAC}}{CN_{BAC}} \tag{P-36}$$

(*continued on next page*)

Table 3 (*continued*)

Lysis:

$$\mathrm{lys_{BAC}} = k_{\mathrm{d}}^{\mathrm{BAC}}\mathrm{BAC}. \tag{P-37}$$

Organic matter
i: (1) quickly biodegradable substrates; (2) slowly biodegradable substrates
Extra-cellular hydrolysis:

$$\mathrm{elys_{D_i}} = e_{\max}^{i}\frac{\mathrm{DC}_i}{\mathrm{DC}_i + k_{\mathrm{d}}^{i}}\mathrm{BAC} \tag{P-38}$$

$$\mathrm{lys_{PC_i}} = k_{\mathrm{b}}^{i}\mathrm{PC}_i; \quad \mathrm{lys_{PN_i}} = k_{\mathrm{b}}^{i}\mathrm{PN}_i; \quad \mathrm{lys_{PP_i}} = k_{\mathrm{b}}^{i}\mathrm{PP}_i. \tag{P-39}$$

Sedimentation:

$$\mathrm{sed_{PC_i}} = k_{\mathrm{sed}}\mathrm{PC}_i; \quad \mathrm{sed_{PN_i}} = k_{\mathrm{sed}}\mathrm{PN}_i; \quad \mathrm{sed_{PP_i}} = k_{\mathrm{sed}}\mathrm{PP}_i \tag{P-40}$$

$$\text{with} \quad k_{\mathrm{sed}} = V_{\mathrm{sed}}/\tfrac{1}{2}\mathrm{WML}_{\mathrm{depth}}$$

Temperature dependence: $p = p'(0.1 + 0.9\mathrm{e}^{T - T^{\mathrm{opt}})^2/\Delta T^2})$ (P-41)

selection is determined at each time step by the minimum function described in Eq. (P-7) (Table 3).

The photosynthetic process φ (Eq. (P-1), Table 3) is governed by the photosynthetically available irradiance (PAR) or I according to the relationship of Platt et al. (1980). It is characterized by three parameters normalized to the functional cellular constituents: (i) the maximal photosynthetic capacity $K_{\max}$, (ii) the photosynthetic efficiency α and (iii) a description of the photoinhibition β. The ambient light I is calculated from (i) the incident PAR I_0 in combination with (ii) ice cover, assuming an albedo of sea-ice and water of 0.95 and 0.15, respectively, and I decreases with depth according to (iii) the Beer–Lambert equation parametrized by the coefficient of vertical light attenuation η (Eq. (P-1), Table 3), which is calculated from phytoplankton biomass according to the empirical relationship determined by Lancelot et al. (1991a) for Antarctic waters. The simple photosynthesis model was preferred to other more sophisticated bio-optical models based on the chlorophyll specific absorption spectrum of phytoplankton and the vertical field of the light spectrum (e.g. Arrigo et al., 1998b; Pondaven et al., 1998), in keeping with the observational data set available for parameterization of photosynthesis by autotrophic flagellates and diatoms.

The synthesis of reserve products s_{R} (Eq. (P-5), Table 3) is governed by the availability of the intracellular monomers S following Michaelis–Menten kinetics characterized by the constants $\rho_{\max}$ (the maximum specific rate of reserve products synthesis R), and k_{S}, the half-saturation constant for the assimilation of S. The catabolism of the reserve products c_{R} is postulated to obey first-order kinetics characterized by the constant $k_{\mathrm{c}}^{\mathrm{R}}$ (Eq. (P-6), Table 3).

The metabolic costs are met primarily by cellular respiration *resp*. This process is expressed by the sum of two terms (Eq. (P-8), Table 3), associated with maintenance processes and the synthesis of new cellular material (Shuter, 1979). Maintenance is

Table 4
SWAMCO model: parameterization

Symbol	Description	Unit	Value	Reference
(a) Phytoplankton dynamics				
State variables: F (functional and structural metabolites), R (reserve products), S (monomers)				
C metabolism				
k_{max}	Photosynthesis optimal specific rate	h^{-1}	0.06	a
α	Photosynthetic efficiency	m^2 s (μmol h)$^{-1}$	0.0007	a
β	Photoinhibition index	m^2 s (μmol h)$^{-1}$	0	a
μ_{max}	Maximum specific rate of F synthesis	h^{-1}	0.035	a
k_s	$\frac{1}{2}$ Saturation constant of S assimilation	mol C (mol C)$^{-1}$	0.07	a
Q_s	Cellular quota of monomeric substrates	mol C (mol C)$^{-1}$	0.07	a
ρ_{max}	Optimal specific rate of R synthesis	h^{-1}	0.06	a
k_c^R	Specific rate of R catabolism	h^{-1}	0.06	a
K_F	Specific rate of maintenance metabolism	h^{-1}	0.0005	a
ecs_{NH_4}	Energy cost of F synthesis (NH_4 source)	mol C (mol C)$^{-1}$	0.4	b
ecs_{NO_3}	Energy cost of F synthesis (NO_3 source)	mol C (mol C)$^{-1}$	0.8	b
k_{lys}	Specific rate of cell autolysis	h^{-1}	0.001	a
ε	Exudation constant	—	0.05	a
V_{sed}	Sedimentation velocity	m h^{-1}	0.035	j
Nutrients uptake				
k_N	$\frac{1}{2}$ Saturation constant for N uptake	mmol N m^{-3}	1	n
k_P	$\frac{1}{2}$ Saturation constant for P uptake	mmol P m^{-3}	0.2	k
k_{Si}	$\frac{1}{2}$ Saturation constant for DSi uptake(DA)	mmol Si m^{-3}	4	c
k_{Fe}^{DA}	$\frac{1}{2}$ Saturation constant for DFe uptake (DA)	μmol Fe m^{-3}	1.2	d
k_{Fe}^{NF}	$\frac{1}{2}$ Sat. const. for Fe uptake (NF)	μmol Fe m^{-3}	0.03	l
I_m	NO_3 Uptake inhibition by NH_4: max. rate	mol N (mol N)$^{-1}$	0.8	e
K_i	NO_3 Uptake inhibition by NH_4: $\frac{1}{2}$ sat. cstant	mmol N m^{-3}	0.45	e
Cellular stoichiometry				
CN_{PHY}	C–F: N ratio*	mol C (mol N)$^{-1}$	5	f
CP_{PHY}	C–F: P ratio*	mol C (mol P)$^{-1}$	80	g
FeC_{DA}	Fe: C–F ratio (diatoms)*	mmol Fe (mol C)$^{-1}$	0.2	i,j
FeC_{NF}	Fe: C–F ratio (nanoflagellates)*	mmol Fe (mol C)$^{-1}$	0.0025	m

(*continued on next page*)

Table 4 (*continued*)

Symbol	Description	Unit	Value	Reference
Φ	Si: C–F dependancy to dissolved Fe (slope)°	mol Si (molC μmol Fe m^{-3})$^{-1}$	− 0.39	h
SiC_0	Si: C–F dependancy to diss. Fe (intercept)°	mol Si (mol C)$^{-1}$	1.52	h
χ	Conversion factor (Chl *a*/C–F)	g Chl *a* (mol C)$^{-1}$	0.5	f
(b) Protozooplankton dynamics				
$graz_{max}^{MCZ}$	MCZ max. specific ingestion rate	h^{-1}	0.02	p
$graz_{max}^{HNF}$	HNF max. specific ingestion rate	h^{-1}	0.03	p
k_g	$\frac{1}{2}$ Saturation constant of ingestion	mmol C m^{-3}	0.25	p
ths_{MCZ}	Prey threshold for food ingestion (MCZ)	mmol C m^{-3}	0.083	p
ths_{HNF}	Prey threshold for food ingestion (HNF)	mmol C m^{-3}	0.33	p
y_{ZOO}	Growth efficiency	Dimensionless	0.38	q
k_d^{ZOO}	Autolysis specific rate	h^{-1}	0.001	r
Cellular stoichiometry				
CN_{ZOO}	C : N ratio	mol C (mol N)$^{-1}$	5	o
CP_{ZOO}	C : P ratio	mol C (mol P)$^{-1}$	80	s
FeC_{ZOO}	Fe : C ratio	mmolFe (mol C)$^{-1}$	0.0024	t
(c) Microbial loop dynamics				
Organic matter dynamics				
ε_d^1	D1 fraction in lysis products	—	0.3	r
ε_d^2	D2 fraction in lysis products	—	0.2	r
ε_p^1	P1 fraction in lysis products	—	0.1	r
ε_p^2	P2 fraction in lysis products	—	0.4	r
k_b^1	P1 hydrolysis rate	h^{-1}	0.005	k
k_b^2	P2 hydrolysis rate	h^{-1}	25×10^{-5}	k
e_{max}^1**	Max. spec. rate of D1 exoenzymatic hydrolysis	h^{-1}	0.75	u
e_{max}^2**	Max. spec. rate of D2 exoenzymatic hydrolysis	h^{-1}	0.25	u
k_d^1	$\frac{1}{2}$ sat. const. For D1 exoenzymatic hydrolysis	mmol C m^{-3}	8.3	u
k_d^2	$\frac{1}{2}$ sat. const. For D2 exoenzymatic hydrolysis	mmol C m^{-3}	83	u
Bacteria metabolism				
b_{max}**	Max. specific rate of BS uptake	h^{-1}	0.18	u
k_{BSC}	$\frac{1}{2}$ saturation constant for BS uptake	mmol C m^{-3}	0.83	u
y_{BAC}	Growth efficiency	—	0.25	x
k_d^{BAC}**	Autolysis specific rate	h^{-1}	0.01	u

Table 4 (*continued*)

Symbol	Description	Unit	Value	Reference
Bacteria stoichiometry				
CN_{BAC}	C : N ratio	mol C (mol N)$^{-1}$	5	[u]
CP_{BAC}	C : P ratio	mol C (mol P)$^{-1}$	80	[w]
FeC_{BAC}	Fe : C ratio	mmolFe (mol C)$^{-1}$	0.0024	[o]
Temperature dependence				
T^{opt}	Optimal temperature	°C	12	[v]
ΔT	Temperature interval	°C	7	[v]

[a]Lancelot et al. (1991a).
[b]Penning De Vries et al. (1974).
[c]Nelson and Tréguer (1992).
[d]Scharek et al. (1997).
[e]Elskens (1998).
[f]Lancelot et al. (1986).
[g]Redfield et al. (1963).
[h]Takeda (1998).
[i]Sunda et al. (1991).
[j]Muggli et al. (1996).
[k]Lancelot et al. (1997).
[l]Price et al. (1994).
[m]Morel et al. (1990).
[n]Adapted from Pondaven et al. (1998).
[o]Tortell et al. (1996).
[p]Becquevort (1999).
[q]Björnsen and Kuparinen (1991).
[r]Adjusted.
[s]Redfield et al. (1963).
[t]Chase and Price (1997).
[u]Billen and Servais (1988).
[v]Billen and Becquevort (1991).
[w]Redfield et al. (1963).
[x]Lancelot et al. (1991b).
*C–F: functional and structural metabolites of phytoplanktonic cells (see Table 1).
**Dependence to temperature expressed as follows: $p = p'(0.1 + 0.9e(T - T^{opt})^2/\Delta T^2)$.

related to the functional cellular biomass according to first-order kinetics parameterized by the constant k_F. Metabolic costs for the synthesis of new cellular material are dependent on the form of the inorganic nitrogen source expressed by the dimensionless constant ξ which is assumed to vary linearly according to the inorganic nitrogen source (Shuter, 1979; Eq. (P-8), Table 3).

The phytoplankton physiological losses include exudation (e) and cell autolysis (lys). The latter process, affecting the whole cell, operates on all phytoplankton state variables including the biogenic silica (BSi) and is described by first-order kinetics parameterized by the constant K_{lys} (Eqs. (P-2) and (P-3), Table 3). The exudation e is a constant fraction ε of photosynthesis φ (Eq. (P-4), Table 3). Sedimentation affects

only the diatoms (Eq. (P-9), Table 3) and biogenic silica (Eq. (P-10), Table 3) and is described by first-order rate parameterized by the constant k_{sed}.

The physiological parameters relevant to phytoplankton growth were determined experimentally by fitting the set of equations (Lancelot et al., 1991, 1997; Mathot et al., 1992) to experimental field ^{14}C data describing the photosynthesis–light relationship and time-course C assimilation in phytoplankton cellular constituents over a 24-h cycle. When conducted at iron-replete concentration, no significant difference in either photosynthetic or growth parameters of the nanophytoplankton-dominant or diatom-dominant communities could be shown (Lancelot et al., 1997). Furthermore, no significant difference in the biochemical composition of controls and iron-enriched field populations has been recorded in iron enrichment bioassay experiments (van Leeuwe et al., 1997). Combining these results allows us to choose just one set of parameters to characterize the carbon metabolism (photosynthesis, growth, respiration, catabolism, exudation) of both phytoplankton groups (Table 4). Furthermore, this set of parameters holds for the whole Southern Ocean because of the lack of significant temperature dependence observed in the range -1.8 and $+3.5$°C (Lancelot et al., 1991a, 1997; Mathot, 1995). Consequently, the physiological growth of diatoms (DA) and nanophytoplankton (NF) in the SWAMCO model is differentiated by the physiology of Fe assimilation, i.e. the differences in cellular Fe requirements and kinetic parameters of Fe uptake. The observed ability of nanophytoplankton to outcompete large diatoms in the low-iron waters of the Southern Ocean has been attributed to their higher affinity for dissolved iron uptake (low K_{Fe}) and their lower biochemical iron requirements (Sunda and Huntsman, 1995; Hutchins, 1995). Half-saturation constants for uptake of dissolved Fe by nanophytoplankton and diatoms were chosen at 0.03 μmol m^{-3} (Price et al., 1994) and 1.2 μmol m^{-3}, respectively (Table 4). The latter concentration was calculated from Fe-enrichment experiments conducted in the Atlantic sector of the Southern Ocean (Scharek et al., 1997; van Leeuwe et al., 1997), assuming that Fe supply in a low Fe environment stimulates only the diatom component of the phytoplankton community. The half-saturation constants are expressed as dissolved Fe to be consistent with the measured dissolved Fe in the ambient seawater during the 1992 campaign (de Baar et al., 1995; Löscher et al., 1997). The role of chemical speciation of the Fe in solution is ignored, because in 1992 this had not yet been investigated. In a subsequent 1995 expedition in the remote Pacific sector (Nolting et al., 1998) the organic complexation of Fe was about 98% leaving only 2% for Fe′, which is the sum of all inorganic Fe(III) species, ignoring reduced Fe(II) forms. When applied to the above K_{Fe} values for the large diatoms this would correspond to a half-saturation value $K_{Fe'}$ of 0.024 μmol m^{-3}. This concentration corresponds well with $K_{Fe'}$ values of order 0.05–0.08 μmol m^{-3} for a large neritic diatom *Chaetoceros calcitrans* grown in the laboratory in EDTA manipulated cultures (Timmermans et al., unpublished results). Otherwise the paradigm of Fe′ being the master variable has arisen from EDTA-manipulated cultures, in which the chemical speciation of Fe has little resemblance to natural seawater (Gerringa et al., 2000). For natural seawater there currently does not yet exist a study in which all the three major forms (Fe′(III), Fe(III)-organic chelates, reduced Fe(II)) have been assessed simultaneously, let alone the availability of one or more of these forms for uptake by

phytoplankton. For example, the recent study (Hutchins et al., 1999) reports that different phytoplankton species apparently prefer different organic chelates of Fe, implicitly suggesting that more than just the inorganic Fe′(III) is affecting plankton growth. Ongoing research of this type, including that in our group, towards unraveling Fe chemical speciation and phytoplankton growth in natural seawater may eventually lead to refinement of ecosystem models like the one here presented.

The cellular Fe requirement (Fe : C) was derived from the literature (Morel et al., 1990; Brand, 1991; Sunda et al., 1991; Muggli et al., 1996) and fixed at 0.2 for diatoms (DA) and 0.0025 mmol : mol nanophytoplankton (NF) (Table 4). The model further considers the negative regulation by ambient Fe of the silicification (Si : C) by diatoms as recently shown by Takeda (1998) and Hutchins and Bruland (1998). The empirical equation described in (P-14) (Table 3) is derived from the bioassay experiments of Takeda (1998) on Antarctic diatoms. Here the term $[\mathrm{Si}:\mathrm{C}]_0$ is the silicification level at depleted Fe, and Φ is the slope of the negative correlation.

The sedimentation rate v_{sed} was fixed at 0.08 m h^{-1} in order to take into consideration an average forcing of Fe stress (Muggli et al., 1996) and aggregation.

2.2.2. *Protozooplankton dynamics*

The marine protozoan community includes a large range of microorganisms which are able to ingest bacteria or auto- and heterotrophic flagellates. Food competitive experiments run on several field communities (Lancelot et al., 1997; Becquevort, 1999) show, however, that the Antarctic protozoan community is highly food selective, allowing it to be represented by two state variables. These are the bactivorous heterotrophic nanoflagellates HNF feeding on the only bacteria BAC and the microzooplankton MCZ grazing on autotrophic (NF) and heterotrophic (HNF) nanoflagellates. The whole community undergoes grazing pressure by metazoans and krill (Eqs. (V-7) and (V-8), Table 2).

The protozoan ingestion rate *graz* (Eqs. (P-17) and (P-25), Table 3) is governed by food availability and obeys Michaelis–Menten kinetics above a threshold value (ths) below which no grazing is likely (Becquevort, 1997). In the absence of food selectivity, the fraction of microzooplankton grazing activity on nanophytoplankton corresponds to the relative abundance of the latter over the total nanoflagellate community (Eqs. (P-17)–(P-19)). A constant fraction y_{zoo} of the ingested food by microzooplankton (MCZ) and bactivorous heterotrophic nanoflagellates (HNF) is converted into biomass (Eqs. (P-16) and (P-24), Table 3), the remaining being respired. The rate of cell autolysis for both groups ($\mathrm{lys}_{\mathrm{MCZ}}$ and $\mathrm{lys}_{\mathrm{HNF}}$ in Eqs. (P-20) and (P-26)) is described by first order kinetics, in which $k_{\mathrm{d}}^{\mathrm{zoo}}$ is a first-order constant. Microzooplankton mortality by grazing corresponds to the part of overall metazoan grazing (considered here as a biological constraint) on microzooplankton (MCZ) with respect to diatoms (DA), in the assumed absence of food selectivity (Eq. (P-30), Table 3).

Protozoan feeding parameters (Table 4) were determined by fitting the process equations to data from kinetic experiments measuring the ingestion rate of natural assemblages of protozoa in the presence of various concentrations of prey (Lancelot et al., 1997; Becquevort, 1999). Half-saturation constants for prey ingestion were remarkably similar for bacterivorous nanoflagellates and microzooplankton, around

0.25 mmol C m^{-3} (Table 4). Unexpectedly, the threshold food concentration below which no grazing was occurring was significantly lower for microzooplankton (MCZ) than for bacterivorous heterotrophic nanoflagellates (HNF), emphasizing a strong coupling between microzooplankton and their prey consisting of both auto- and heterotrophic nanoflagellates (NF and HNF). The common value of 0.38 was considered as typical for the growth efficiency of Antarctic protozoa (Björnsen and Kuparinen, 1991).

2.2.3. Microbial loop dynamics

The model of organic matter degradation by bacteria considers one single bacterioplankton group BAC (including both free-living and attached bacteria on particles and aggregates) and five pools of organic substrates (the monomeric substrates for bacteria BS; the rapidly biodegradable dissolved and particulate organic matter D_1 and P_1; the slowly biodegradable dissolved and particulate organic matter D_2 and P_2). The growth of the bacteria is directly dependent on the concentration of their substrate (BS), the organic monomers available for transfer into bacteria. These monomers are supplied either directly by phytoplankton exudation or indirectly after bacterial ectoenzymatic hydrolysis of the dissolved and particulate polymers (D_i, P_i). The elemental composition of organic polymers includes carbon (DC; PC_i), nitrogen (DN_i; PN_i) and phosphorus (DP_i; PP_i). That of the monomers include carbon (BSC) and nitrogen (BSN). Conservation equations are listed in Table 2 (Eqs. (V-9)–(V-17).

The dissolved and particulate polymers (D_i and P_i) are supplied by lysis of phytoplankton, bacteria and protozoa. The model defines as ε_d^i and ε_p^i the fractions of D_i and P_i of the bulk of organic matter released by lysis (Eqs. (V-12)–(V-17), Table 2). The hydrolysis rate of particulate polymers lys_{Pi} (Eq. (P-39), Table 3) is described by first-order kinetics characterized by 2 constants k_b^1 and k_b^2. The involvement of attached bacteria in this process is indirectly considered by assuming a temperature dependence for the hydrolysis constant k_b' such as described in Eq. (P-41) (Table 3). The ectoenzymatic hydrolysis $elys\ D_i$ of dissolved organic polymers (Eq. (P-38), Table 3) obeys a Michaelis–Menten kinetics (Somville and Billen, 1983) characterized by two sets of two specific parameters (the maximum specific rate of ectoenzymatic hydrolysis e_{max}^i and the half-saturation constant k_D^i for hydrolysis of D_i), owing to the different susceptibilities to enzymatic hydrolysis of the two classes of dissolved polymers (Billen, 1990).

The bacterial uptake of monomeric substrates (BS) upt_{BAC} is assumed to obey Michaelis–Menten kinetics (Eq. (P-33), Table 3) where b_{max} and k_{SBC} are the maximum specific rate and half-saturation constant of substrate uptake by bacteria. A constant fraction y_{BAC} of the amount of substrates taken up is used for biomass production (Eq. (P-32), Table 3), the remaining part being respired and remineralized.

Parameters were determined experimentally (Billen and Becquevort, 1991; Lancelot et al., 1991b; Servais et al., 1987). Values are reported in Table 4. Contrasting with eukaryotic cells, bacterial activity in the Southern Ocean was found to be governed by ambient temperature according to the sigmoid relationship (Eq. (P-41), Table 3) described in Billen and Becquevort (1991).

2.2.4. Inorganic nutrients loop

Nitrate, ammonium, phosphate, iron and silicate (NO_3, NH_4, PO_4, DFe and DSi) are the inorganic nutrients considered by the model (Eqs. (V-18)–(V-23), Table 2). Both algal groups, the diatoms and the nanoflagellates, take up nitrate, preferably ammonia, phosphate and iron, all to be assimilated into the only functional constituents F (Lancelot et al., 1986). The ratio of phytoplankton nitrate uptake to the total inorganic N uptake (f_{NO_3}; (Eq. (P-11) in Table 3) is governed by ammonia according to the non-competitive inhibition equation suggested by Harrison et al. (1996) and parameterized by Elskens et al. (1997), (Table 4). Silicate is used only by the diatoms and is released into the surrounding medium after diatom autolysis. Uptake rates of N, P, Si and Fe (Eqs. (P-11)–(P-15), Table 3) are deduced from the computed phytoplankton growth rate (Eq. (P-7), Table 3) and the cellular stoichiometry of diatoms and nanophytoplankton (Table 4). Iron and phosphorus requirements of the bacteria are met by direct uptake of both nutrients. In contrast, NH_4 can be either taken up or released by bacteria according to the N : C ratio of their substrates and their own biochemical requirements (Eq. (P-36), Table 3). The ammonia, phosphate and iron are released by protozoa as products of their metabolism (Hutchins et al., 1995). Regenerating processes are computed by comparing the N, P and Fe content of food resources with their biochemical requirements (Eqs. (P-21)–(P-23), Eqs. (P-27)–(P-29), Table 3). Autolysis of micro-organisms further releases iron into the surrounding medium (Eq. (V-23), Table 2). Stoichiometric ratios (Fe : N : Si : C) were derived from literature values (Morel et al., 1990; Chase and Price, 1997; Sunda and Huntsman, 1997; Tortell et al., 1996) and are reported in Table 4 for phytoplankton, protozooplankton and bacterioplankton.

3. Model results: application to the conditions of ANTX/6 cruise of RV *Polarstern*

3.1. The 1992 spring bloom in the Atlantic sector of the Southern Ocean

The ANTX/6 sampling site at 6°W and between 48 and 60° S in the Atlantic sector of the Southern Ocean is crossed by two eastward flowing but contrasting water masses (de Baar et al., 1995; Veth et al., 1997). These are the iron-depleted ($\sim$0.4 nM) but sea-ice-associated southern branch of the Antarctic Circumpolar Current ACC ($\sim$ 51–56°S) and the iron-enriched (1.8 nM) Polar Frontal region PFr ($\sim$47–50°S). Transects extending from the ice edge of the eastern Weddell Sea, across the southern branch of the ACC into the Polar Front had repeatedly been sampled over more than a one-month period (Fig. 2), at the early beginning of the 1992 growth season. Meteorological conditions were severe in particular during the first half of the cruise, when storm events with wind velocities higher than 15 m s^{-1} were frequent (Fig. 3a). Results are well documented [see the special issue of DSR Part II, 44(1–2) edited by Smetacek et al., 1997a,b] and include a large data set (Rommets et al., 1997) of spatio-temporal distributions of inorganic nutrients and dissolved iron (Löscher et al., 1997), Chl *a* (Bathmann et al., 1997), biogenic silica (Quéguiner et al., 1997), diatoms and nanophytoplankton (Bathmann et al., 1997), bacteria (Lochte et al., 1997),

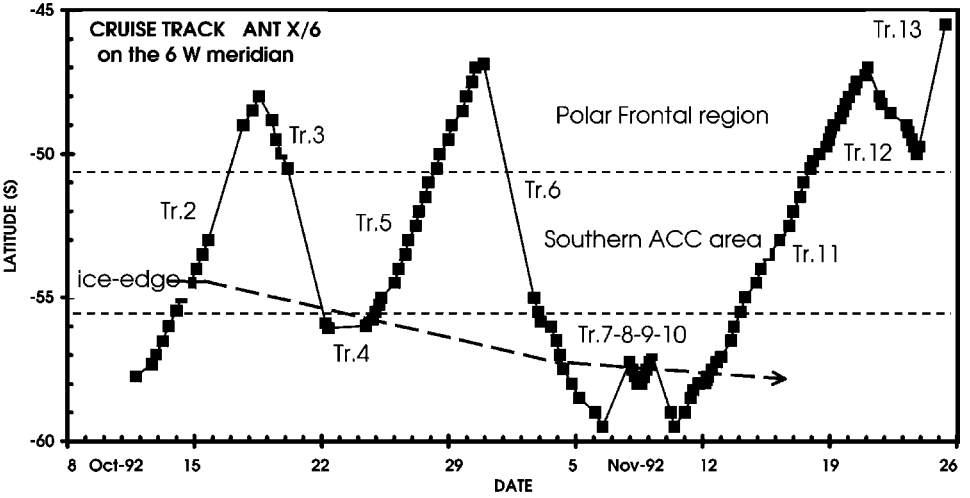

Fig. 2. Latitude vs. time cruise track on the 6°W meridian of ANT X/6 aboard R.V. *Polarstern*. Transects number and the change in ice-edge position are indicated.

microzooplankton (Becquevort, 1997) and metazooplankton (Fransz and Gonzales, 1997; Dubischar and Bathmann, 1997) that can be used for comparison with model results.

One of the major findings of the cruise was the negligible build-up of phytoplankton biomass at the retreating ice-edge. Chl *a* concentrations were significantly less than 1 mg m^{-3} (Bathmann et al., 1997). The spring microbial community was organized in a complex microbial network composed of autotrophic nanoflagellates, bacteria, bactivorous (heterotrophic flagellates) and protistovorous protozoa (microprotozoa) of low and relatively stable biomass (Becquevort, 1997). This was in contrast with the Polar Frontal region where concentrations of Chl *a* as high as 3 mg m^{-3} were observed at the end of the sampling period (Bathmann et al., 1997), when meteorological conditions were improving (Fig. 3a). In this region Chl *a* increased from 0.6–1.6 to 1.2–2.4 mg m^{-3} within about three weeks, while dissolved iron exhibited a concomitant seasonal decrease of almost 1 μmol m^{-3} (de Baar et al., 1995). Elevated rates of primary production between 80 and 250 mmol C m^{-2} d^{-1}, mostly synthesized by the largest (> 20 μm) phytoplankton, were measured (Jochem et al., 1995), and the phytoplankton community was dominated by neritic diatoms such as *Corethron criophilum* and *Fragilariopsis kerguelensis* (Veth et al., 1997). Accordingly, significant export production of particulate carbon had been estimated in this area from ^{234}Th deficiencies (Rutgers van der Loeff et al., 1997).

3.2. SWAMCO model implementation

For its application in the Antarctic Circumpolar Current during the 1992 cruise ANTX/6 of RV *Polarstern*, the SWAMCO model was coupled with a one-dimensional

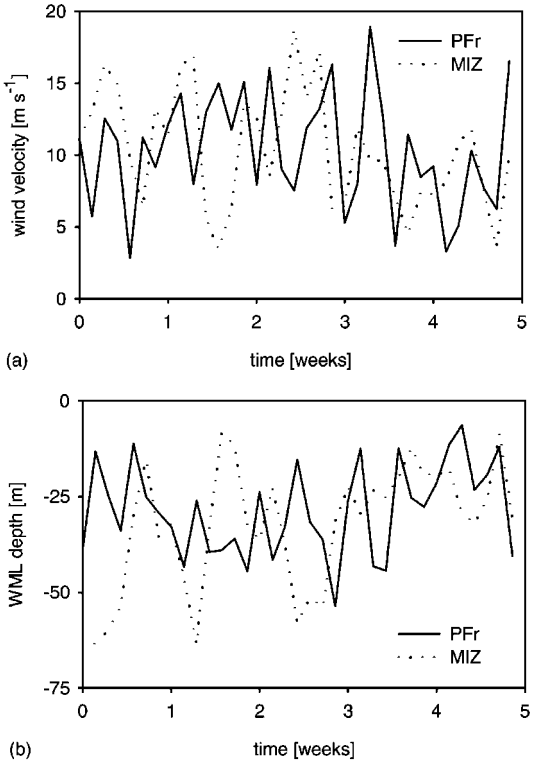

Fig. 3. Evolution of in situ wind speed (a) and simulated wind mixed layer depth (b) in the Polar Frontal region (PFr, at 48°S) and the marginal ice zone (MIZ, at 56°S) over the period of the ANT X/6 cruise.

hydrodynamical model. The general frame work consists of a two-layer 1-D model composed of a well-mixed upper layer and a stratified deeper layer down to the euphotic depth at 100 m (Lancelot et al., 1993). Such a low resolution of physical processes is reasonable as horizontal advection (about 300 km over the 40 day-modeling period) is of low significance in comparison with changes in the pattern of atmospheric forcing. The hydrodynamical model is an adaptation to polar seas of the wind-mixed layer model of Denman (1973). The numerical code was extended with terms describing freshwater fluxes from ice melting and the effects of wind friction changes over ice-covered regions. Basic concepts, mathematical description and parameterization are described extensively by Veth (1991a, b). Performance and limits of the model are discussed by Veth et al. (1992).

The 1D-SWAMCO model was tested by running simulations over the 40 d cruise period (20 October–30 November 1992) and for the physico-chemical conditions covering latitudes between 47°S and 58°S, with a half-degree definition. The sea ice conditions, irradiance and meteorological data reconstructed from continuous ship-board measurements and satellite information were used as physical forcing functions. Metazoan grazing pressure was disregarded for this application because of its

Table 5
SWAMCO model: Initial conditions of phytoplankton, protozooplankton, bacteria, organic matter and nutrients for the 3 investigated hydrographic regions (Polar Frontal region, ice-free Southern ACC, Marginal Ice Zone). Data are surface waters averaged concentrations recorded along the first transect (Tr. 2, Fig. 2), extracted from the CD-ROM database of the JGOFS ANT X/6 cruise (Rommets et al., 1997)

State variable	Hydrographic region			
	Unit	PFr	SACC	MIZ
Phytoplankton				
Diatoms	mg Chl *a* m^{-3}	0.33	0.14	0.03
Nanoflagellates	mg Chl *a* m^{-3}	0.17	0.19	0.19
Protozooplankton				
microzooplankton	mmol C m^{-3}	0.36	0.26	0.18
Heterotrophic nanoflagellates	mmol C m^{-3}	0.08	0.07	0.06
Bacteria	mmol C m^{-3}	1.16	0.30	0.28
Organic matter				
Dissolved organic carbon	mmol C m^{-3}	16.6	16.6	16.6
Particulate organic carbon	mmol C m^{-3}	0.5	0.5	0.5
Dissolved organic nitrogen	mmol N m^{-3}	1.9	1.9	1.9
Particulate organic nitrogen	mmol N m^{-3}	0.1	0.1	0.1
Nutrients				
Nitrate	mmol N m^{-3}	25.1	27.1	28.3
Ammonium	mmol N m^{-3}	0.10	0.19	0.11
Phosphate	mmol P m^{-3}	1.7	1.9	1.9
Silicic acid	mmol Si m^{-3}	20.2	36.6	55.7
Dissolved iron	μmol Fe m^{-3}	1.8	0.49	0.40

negligible contribution at this period of the year (Dubischar and Bathmann, 1997). The temporal variation of the state variables was calculated by integrating the differential equations of the model (Table 2, Eqs. (V-1)–(V-23)) according to the Runge–Kutta fourth order procedure, with a step of 30 min and to a depth of 100 m. The vertical resolution is one meter. The values of the state variables within the upper mixed layer were averaged at each time step. Initial values of chemical and biological state variables (Table 5) were those observed at the first cross-section (Transect 2, Fig. 2) and were extracted from the database of Rommets et al. (1997).

3.3. 1D-SWAMCO model results

3.3.1. Time evolution of wind mixed layer depth and surface layer nutrients and phytoplankton in the Polar Frontal region and at the receding ice-edge

The ability of the SWAMCO model to reproduce the contrasting phytoplankton bloom conditions recorded in spring 1992 in the Polar Frontal region and at the receding ice edge (Marginal Ice Zone, MIZ) was first appraised by comparing model simulations at 48 and 56°S (Figs. 3 and 4) latitude. Fig. 3b shows the daily evolution of

Fig. 4. SWAMCO model predictions of diatom-Chl *a* (a), nanoflagellate-Chl *a* (b), nitrate (c), ammonium (d), silicic acid (e), dissolved iron (f), phosphate (g), POC (h) in the Polar Front region (PFr), and the marginal ice zone (MIZ) over the period of the ANT X/6 cruise.

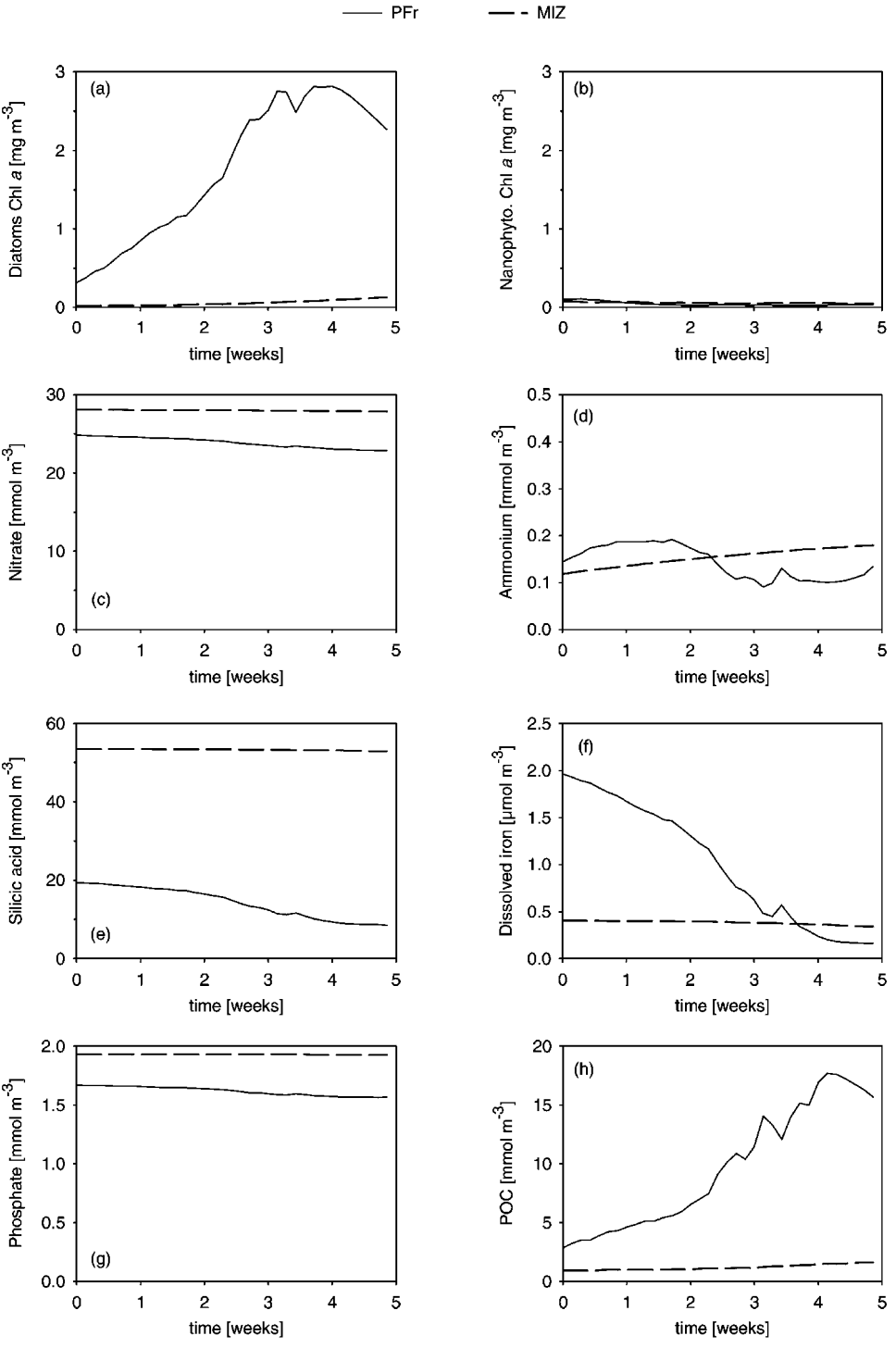
PFr
MIZ
(a)
Diatoms Chl a [mg m-3]
(b)
Nanophyto. Chl a [mg m-3]
(c)
Nitrate [mmol m-3]
(d)
Ammonium [mmol m-3]
(e)
Silicic acid [mmol m-3]
(f)
Dissolved iron [µmol m-3]
(g)
Phosphate [mmol m-3]
(h)
POC [mmol m-3]
time [weeks]

the depth of the upper mixed layer over the 40-d cruise period as predicted by running the physical model under in situ meteorological forcing (Fig. 3a). Similar high fluctuations of the wind mixed layer depth (between 10 and 60 m; Fig. 3b) are predicted at both latitudes in response to frequent events of extreme wind (Fig. 3a), while predicted deep wind mixing events are more intense during the first three weeks of the simulated period (Fig. 3b). Also a deeper convection is generally predicted at latitude 56°S, due to the combination of higher winds (Fig. 3a) and sea-ice cooling. At both latitudes a more stable surface layer of about 20 m is predicted during the final ten days of the simulated period (Fig. 3b) coinciding with a lower average wind speed (~ 7 m s^{-1}) and a decrease of storm frequency (Fig. 3a). The light and iron co-limitation of diatom growth is shown by comparing 1D-SWAMCO simulations of diatom-Chl *a* (Fig. 4a), dissolved Fe (Fig. 4f) and wind mixed layer depth (Fig. 3b) at both latitudes. In agreement with observations (Bathmann et al., 1997; Veth et al., 1997), a significant diatom build-up, reaching 2.8 mg Chl *a* m^{-3}, is simulated in the surface layer of the iron-enriched 48°S latitude (Fig. 4a). Maximum Chl *a* concentrations are predicted at the end of the simulated period, when ambient light is optimal because of the increased stability of the surface layer (Fig. 3b). Concomitant with the increase of diatom-Chl a the model predicts decreases of silicate, nitrate and iron of 10 mmol m^{-3} (Fig. 4e), 3 mmol m^{-3} (Fig. 4c) and 1.8 μmol m^{-3} (Fig. 4f). The simulated imbalance between the nitrate and silicate drop (Figs. 4c and e) fits perfectly with observations at the Polar Front (de Baar et al., 1997) and most likely reflects the iron dependence of the diatom silicification considered in the SWAMCO model (Table 4a). The diatom decline of 0.5 mg Chl *a* m^{-3} predicted at the end of the simulated period (Fig. 4a) reflects shortage of dissolved iron (0.16 μmol m^{-3}; Fig. 4f) under optimal light conditions (Fig. 3b). As expected from field observations (Veth et al., 1997) no real diatom bloom is simulated in the iron-deficient ice-covered region where predicted diatom-Chl *a* remains at concentration less than 0.1 mg m^{-3} (Fig. 4a). Still a slight increase of diatom-Chl *a* is predicted at the end of the simulated period coinciding with disappearance of the sea-ice and an enhanced vertical stability (Fig. 3b). This diatom build-up (0.1 mg Chl *a* m^{-3}) under optimal light conditions remains trivial, though, because of growth limitation by the low ambient dissolved iron (Fig. 4f). Interestingly, the time evolution of predicted nanophytoplankton-Chl *a* is constant and similar for both latitudes (Fig. 4b). The low and unchanging concentrations of its Chl *a* (less than 0.1 mg Chl *a* m^{-3}; Fig. 4b) predicted under the varied conditions of light and iron reflect the grazer control of autotrophic nanoflagellates.

3.3.2. Geographical variations of nutrients and phytoplankton along Transect 11

The overall performance of the SWAMCO model was best assessed by reconstructing transect 11 of the cruise track (Fig. 2) from the model predictions of dissolved inorganic nutrients and Chl *a* averaged within the upper mixed layer and comparing them with the corresponding field observations (Fig. 5). Transect 11 was chosen because at that time the phytoplankton distribution was more geographically contrasted and a noticeable diatom bloom was recorded in the Polar Frontal region (Fig. 5a). Fairly good agreement is reached between predictions and available observations (Fig. 5). The model simulates remarkably well the observed geographical distribution

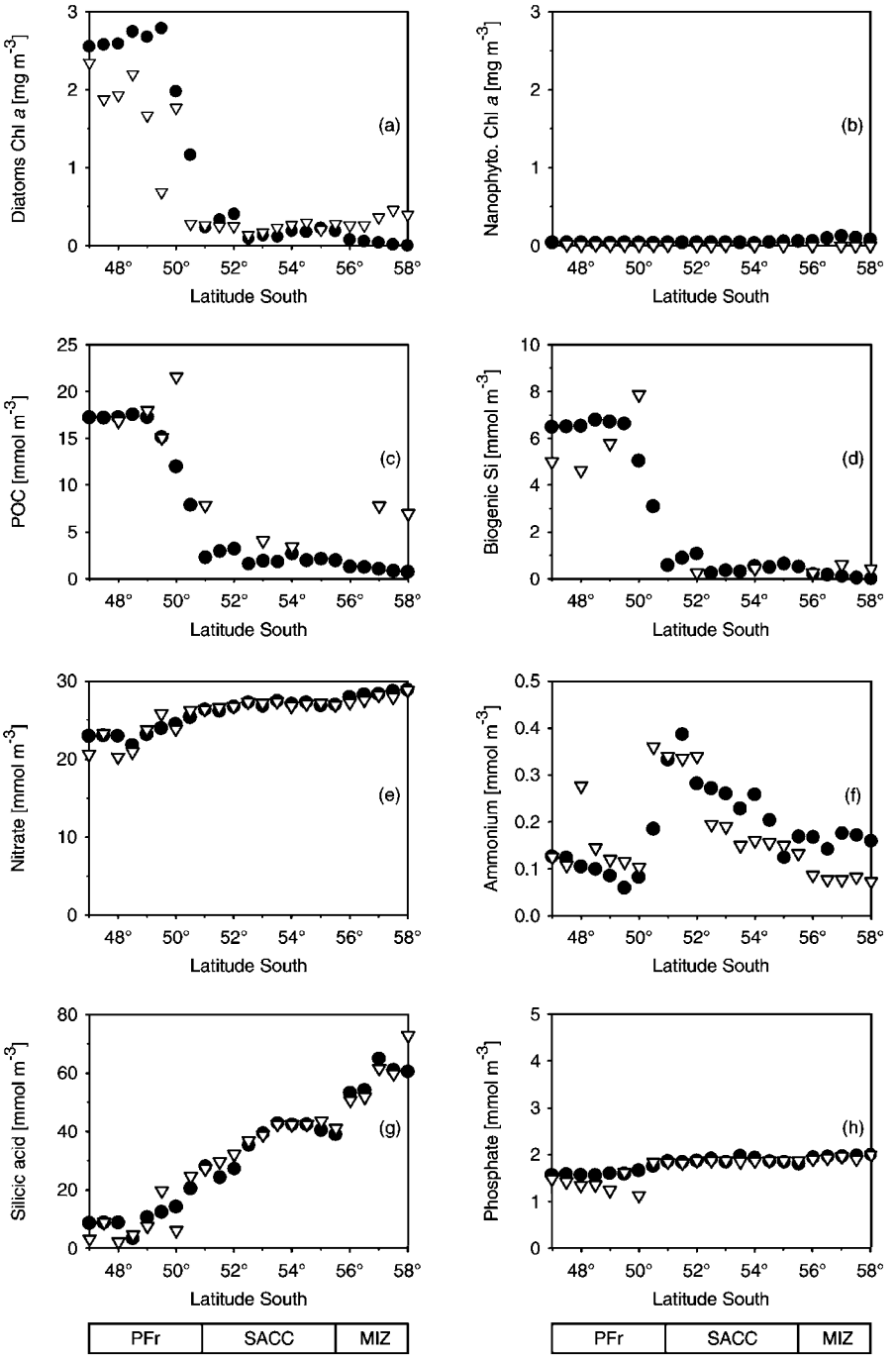

Fig. 5. SWAMCO model predictions (●) vs. field observations (▽) along transect 11 of the ANT X/6 cruise of diatom-Chl *a* (a), nanoflagellate-Chl *a* (b), POC (c), biogenic silica (d), nitrate (e), ammonium (f), silicic acid (g), phosphate (h).

of Chl *a* characterized by elevated concentrations at the Polar Front (Fig. 5a) and the lack of phytoplankton build up at the receding ice-edge (Fig. 5b). More than 90% of the predicted phytoplankton biomass in the Polar Frontal region is diatoms (Fig. 5a), with negligible contribution of nanophytoplankton (Fig. 5b). The model predicts an increase of diatomaceous Chl *a* of 1.8 mg m^{-3} over the one-month simulated period. This corresponds to a predicted accumulation of 2.5–2.8 mg Chl *a* m^{-3} (Fig. 5a) and of about 7 mmol m^{-3} biogenic silica (Fig. 5d), both of which compare very well with field measurements (Bathmann et al., 1997; Quéguiner et al., 1997). Significant decreases of dissolved iron and silicate of 1.7 μmol m^{-3} and 10 mmol m^{-3} (Figs. 4e and f) but negligible decreases of nitrate (2 mmol m^{-3}; Fig. 4c) and ammonium (0.1 mmol m^{-3}; Fig. 4d) are simulated for the same period. Altogether these nutrient simulations are in fine agreement with field data from the Polar Front (de Baar et al., 1997; Löscher et al., 1997; Quéguiner et al., 1997). Model predictions show clearly that depletions of both dissolved Fe and Si are associated with the diatom bloom in the Polar Frontal region, while nitrates are little used and never depleted (Fig. 5e). This gives a computed NO_3 : DSi drawdown of 0.22 for the duration (40 d) of the ANT X/6 cruise, very close to that calculated from nutrient vertical profiles (0.27; Löscher et al., 1997). Such a low NO_3 : DSi consumption ratio explains the observed and simulated shift in the molar NO_3 : DSi signature of surface layer from $\sim$1 (1.2) in winter towards $\sim$3 at the end of the simulated period. In contrast the predicted NO_3 : PO_4 drawdown occurs at a molar ratio of 14.5, close to Redfield et al. (1963), in close agreement with observations (14.2; Löscher et al., 1997), and not very far from the averaged value for the entire vegetative season in the Weddell Sea (15.2; Hoppema and Goeyens, 1999). Altogether these simulations give support to the statement that summer 'NO_3-replete–DSi-depleted' oceanic surface waters could be a reliable diagnostic indicator of Fe-limited upwelled waters.

On the other hand, the model predicts low (0.1–0.2 mg Chl *a* m^{-3}) to negligible (< 0.1 mg Chl *a* m^{-3}) phytoplankton biomass in the iron-depleted waters of the ice-free southern ACC (sACC) and the Marginal Ice Zone (MIZ) (Figs. 5a and b). Interestingly and in accordance with the field data (Bathmann et al., 1997; Becquevort, 1997), the predicted phytoplankton community is dominated by nanophytoplankton in the MIZ and by diatoms in the sACC area (Figs. 5a and b). Accordingly, only a modest increase of biogenic silica is predicted in the ice-free sACC (Fig. 5d), which agrees with field measurements (Quéguiner et al., 1997).

4. Discussion

4.1. Food web structure and particulate export production in the surface layer of the PFr and sACC in spring 1992

4.1.1. Iron availability and food web structure

The role of iron in structuring the Antarctic food web was investigated by comparing the budgets of C, N and Fe in the surface layer as calculated from SWAMCO predictions in the iron-enriched PFr (48°S) and iron-depleted MIZ (56°S) for the 1992 spring period (Fig. 6). One major result of this calculation is the occurrence at both

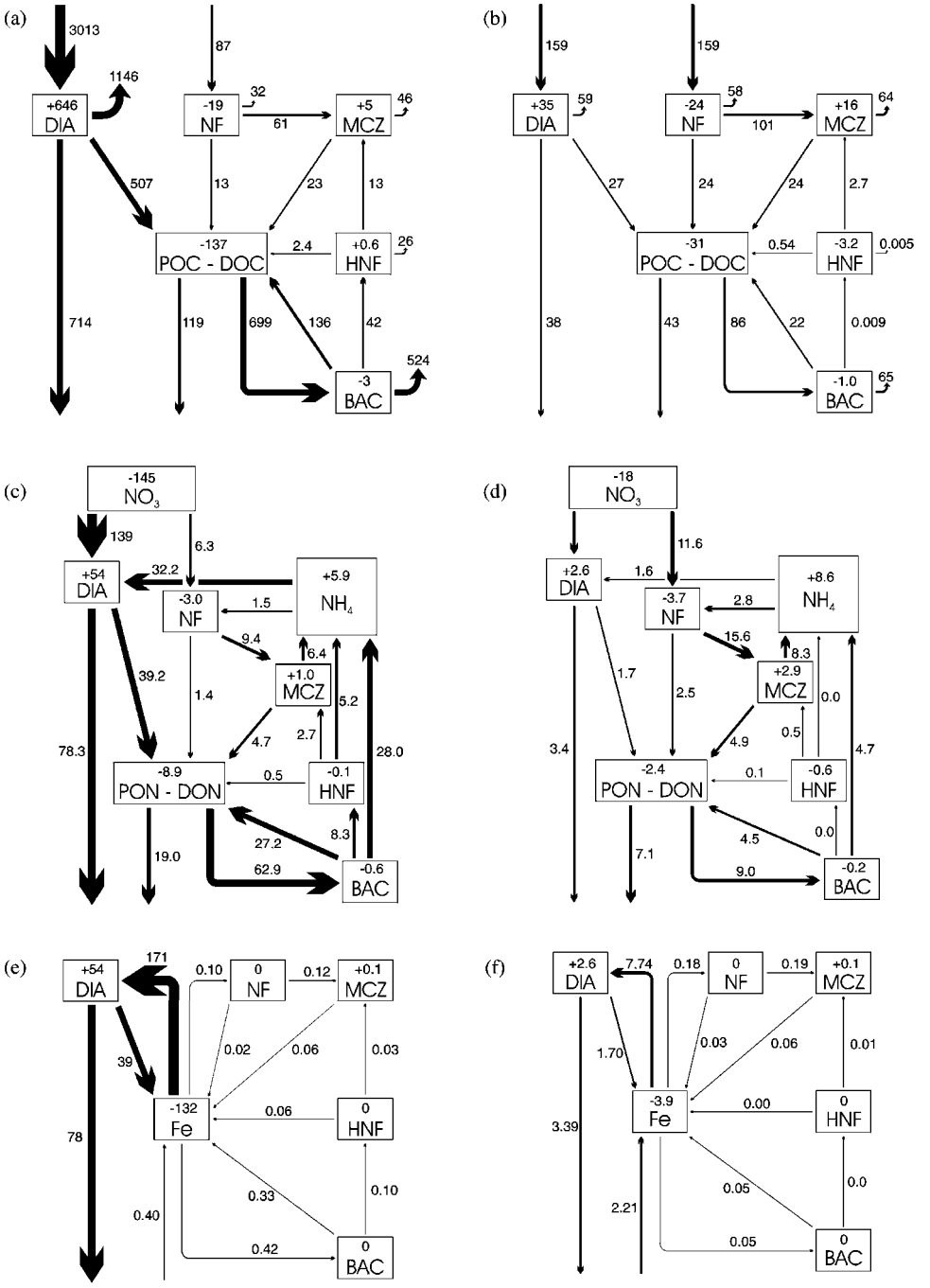

Fig. 6. SWAMCO model prediction of carbon (a, b), nitrogen (c, d) and iron (e, f) budgets within the upper layer (100 m) of the Polar Front region (a, c, e) and the marginal ice zone (b, d, f) integrated over the period of the ANT X/6 cruise. Units: mmol C m^{-2} (a, b), mmol N m^{-2} (c, d), μmol Fe m^{-2} (e, f).

latitudes of a common basal microbial food chain proceeding at about the same rate, independent of iron and light availability. In both areas, nanophytoplankton are heavily controlled by microzooplankton, which ingest more than 95% of the net nanophytoplankton production (Figs. 6a and b). The strong coupling between nanophytoplankton iron uptake and regeneration from microzooplankton catabolic activity (Figs. 6e and f) suggests that the microbial food chain is sustained by regenerated iron. Surprisingly, the model predicts that nitrate rather than ammonium fulfills the nitrogen needs of nanophytoplankton (Figs. 6c and d). We estimate a value of ~ 0.8 for f_{NO_3} (the ratio between nitrate uptake and inorganic N uptake) of nanophytoplankton production. Such a high f_{NO_3} argues against an ammonia regeneration-based microbial food web (Goeyens et al., 1992) but agrees with the view of a nitrate-based late winter-early spring production (Kristiansen et al., 1992). Predicted diatom production in the MIZ is as low as that of the grazer-controlled nanophytoplankton (0.16 mol C m^{-2}; Fig. 6b) with resulting negligible export production of C and biogenic elements (Figs. 6b, d and f). In contrast, in the iron-enriched Polar Frontal region, a significant diatom production of 1.8 mol C m^{-2} (Fig. 6a) controlled by new sources of iron (Fig. 6e) and sustained by nitrates as the nitrogen source (Fig. 6c) is superimposed on the basal microbial food chain. In the absence of mesograzers the model predicts that 25% of the photo-assimilated carbon (0.7 mol m^{-2}; Fig. 6a) and about 50% of the nitrate (0.09 mol m^{-2}; Fig. 6c) and iron (0.09 mmol m^{-2}; Fig. 6e) assimilated by diatoms are directly exported from the surface layer to the deep ocean. The remaining production is accumulated in the surface layer, partly as diatom biomass and partly as particulate and dissolved organic matter supplied by the lysis of ungrazed diatoms. The latter process clearly enhances bacterial production by one order of magnitude compared to that computed for the MIZ bacteria (Figs. 6a and b) and fuels the microbial network through the grazing of the bactivorous heterotrophic flagellates (Fig. 6a). Altogether the model predicts that the bacterial pathway fuels 17% of microzooplankton grazing (Fig. 6a).

4.1.2. Diatom blooms and particulate export production

Export production out of the upper 100 m of particulate carbon and nutrient elements were calculated from SWAMCO model runs for the ANTX/6 cruise period. Results of this calculation are given for three distinct areas: the iron-enriched PFr, the ice-free sACC and the MIZ. The last two have low ambient iron but contrasting phytoplankton dominance (Fig. 5). For all 3 regions the modeled export was compared with independent estimates based on field measurements (Table 6).

The predictions of particulate carbon export compare quite fairly with the estimates derived from deficiencies of the inventories of the natural tracer ^{234}Th (Rutgers van der Loeff et al., 1997) within the Polar Front and the southern branch of the ACC (Table 6). The estimates from ^{234}Th in units of carbon depend strongly on the adopted conversion factor for ^{234}Th : C, which has considerable uncertainty (Rutgers van der Loeff et al., 1997) giving rise to the reported ranges of field values (Table 6). Otherwise the SWAMCO predictions are within or near these ranges and thus confirm that events of high particulate export production are associated with diatom production that occurred in the Polar Front during the second half of the cruise, when

Table 6
Primary production and export production integrated over the period of the ANT X/6 cruise, for three contrasting hydrographic regions (Polar Frontal region, ice-free Southern ACC, Marginal Ice Zone). Units: mmol m^{-2} (except elemental ratios)

		Hydrographic region		
		PFr	SACC	MIZ
(a) *SWAMCO predictions*				
Primary production		1923	459	200
Export production				
Particulate organic carbon		833	143	81
Particulate organic carbon (% primary production)		43.3	31.2	40.5
Particulate organic nitrogen		97	16	11
Opal		446	55	24
Iron		0.078	0.008	0.003
C : N [mol C : mol N]		8.6	8.8	7.7
Si : C [mol Si : mol C]		0.54	0.38	0.30
Fe : C [mmol Fe : mol C]		0.09	0.05	0.04
(b) *Comparison between SWAMCO predictions and field estimations*				
Primary production	SWAMCO	1923	459	200
	^{14}C incubations[a]	2449	456	389
Carbon export production	SWAMCO	833	143	81
	^{234}Th[b]	430–860	150–310	120–240
	O_2 consumption (Ba)[c]	228	145	91

[a]Jochem et al. (1995).
[b]Rutgers van der Loeff et al. (1997).
[c]De hairs et al. (1997).

meteorological conditions were favorable (Figs. 3 and 5). As calculated by Rutgers van der Loeff et al. (1997), the predicted C export production is significantly higher in the iron-enriched PFr than in the sACC and MIZ. When compared with the level of primary production, however, the percentage of particulate C export is about 40% (Table 6) and does not differ much between areas. This would suggest that the algal concentration reached by the Polar Front bloom of 1992 was below the critical level for physical aggregation of phytoplankton and the formation of rapidly sinking aggregates (Jackson, 1990)

Opal export production in the upper 100 m, calculated similarly from model runs, provides additional evidence of the role of diatom blooms in driving particulate export production. Predicted opal export production in the PFr is one order of magnitude higher than in the sACC and MIZ (Table 6). Also iron export production is strongly associated with the bloom of diatoms, which exports 44% of the iron assimilated by the diatom community in the upper 100 m (Table 6). Altogether the computed Si : C, N : C and Fe : C ratios indicate regional difference in the quality of the exported material. This material is significantly enriched in silicon and iron in the PFr compared to the sACC and MIZ (Table 6). The high particulate Si : C ratio in the

Polar Front region is expected to enhance the settling velocity (Muggli et al., 1996), hence enhance the transfer of heavy diatom-derived material from the surface waters into the deep ocean and the sediments. Such more rapid settling would help to minimize the bacterial degradation and mineralisation that occur during this transfer. Indeed evidence for undegraded diatom material reaching the sediments has recently been reported elsewhere in the Southern Ocean (Fileman et al., 1998). In our region indirect estimates of the subsurface (200–400m-intermediate layer) mineralisation rates computed from vertical profiles of barium and oxygen consumption are given by Dehairs et al. (1997); see our Table 6. Combining values of Table 6 with SWAMCO predictions indicates that export production within the sACC and MIZ is almost totally remineralised below 400 m. In the PFr, only 36% of the production exported from the surface layer is remineralised within the first 400 m; the remainder, about 0.5 mol m^{-2}, is exported into the deep ocean. Interestingly the latter number compares fairly well with the annual carbon export production of 0.75 mol C m^{-2} estimated in this region from the accumulation of excess barium in the sediments (Dehairs et al., unpublished results). This comparison provides additional support to the important role of episodic diatom blooms in driving export production from the surface waters to the sediment.

4.2. Sensitivity testing based on SWAMCO model scenarios

4.2.1. Iron enrichment scenarios

Current knowledge of the structure and functioning of the Antarctic food chain (de Baar and Boyd, 1999; Lancelot et al., 1993; Lancelot et al., 1997) suggests that the timing, the amplitude and the extent of Antarctic diatom blooms are determined by the combined action of the light environment, under control of sea ice and wind stress; grazing pressure by micro- and mesozooplankton and krill; and iron availability. The interplay among these factors is however not unique over the whole Southern Ocean, either temporally or geographically. The successful application of the SWAMCO model to the sampling section of the cruise ANTX/6 of R/V Polarstern in the Atlantic sector of the Southern Ocean indicates that the model is able to properly integrate the complex interactions between physical, chemical and biological factors as co-limiting agents of diatom bloom developments and food-web structures. Next, the dual role of iron and light in driving the magnitude of diatom blooms and of export production was investigated by testing the response of the SWAMCO model to iron-enrichment scenarios simulating several continuous atmospheric inputs under the in situ meteorological forcing. These scenarios were conducted at two contrasted latitudes: 48°S in the iron-enriched and ice-free Polar Front region (Fig. 7) and 56°S in the iron-depleted marginal ice zone of the sACC (Fig. 8).

Model simulations over the 40-d period clearly shown the key role of Fe availability and meteorological conditions in driving diatom blooms and carbon export production (Figs. 7 and 8). No effect of iron enrichment on diatom growth is predicted at either latitude during the two first weeks of the simulation (Figs. 7 and 8). The frequent deep mixing events prevailing during this period (Fig. 3b) prevent any bloom development no matter how much iron is added. This light limitation effect is exacerbated by

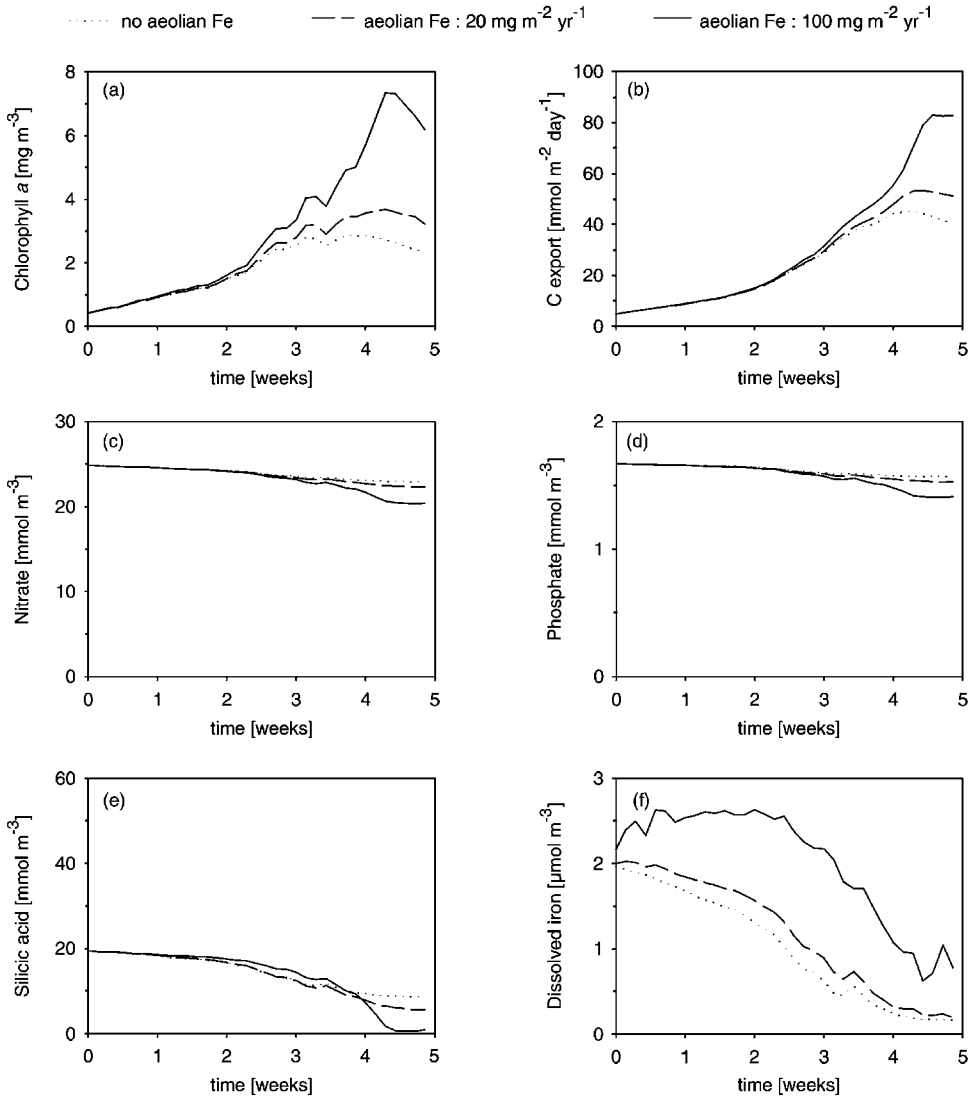

Fig. 7. SWAMCO model response of diatom-Chl *a* (a), carbon export production (b), nitrate (c), phosphate (d), silicic acid (e), and dissolved iron (f) to continuous atmospheric inputs of iron (0–100 mg m^{-2} yr^{-1}) in the Polar Front region (PFr) over the period of the ANT X/6 cruise.

the presence of ice cover at latitude 56°S, slowing down dramatically the build up of diatoms. The maximum effect of iron enrichment on diatom blooms is predicted during the last 10 d of the simulation (Figs. 7 and 8), when favorable meteorological conditions are reached and maintained (wind speed less than 10 m s^{-1}; Fig. 3a). Under such conditions of enhanced vertical stability, the predicted maximum biomass reached by the diatom bloom is obviously determined by the magnitude of the iron

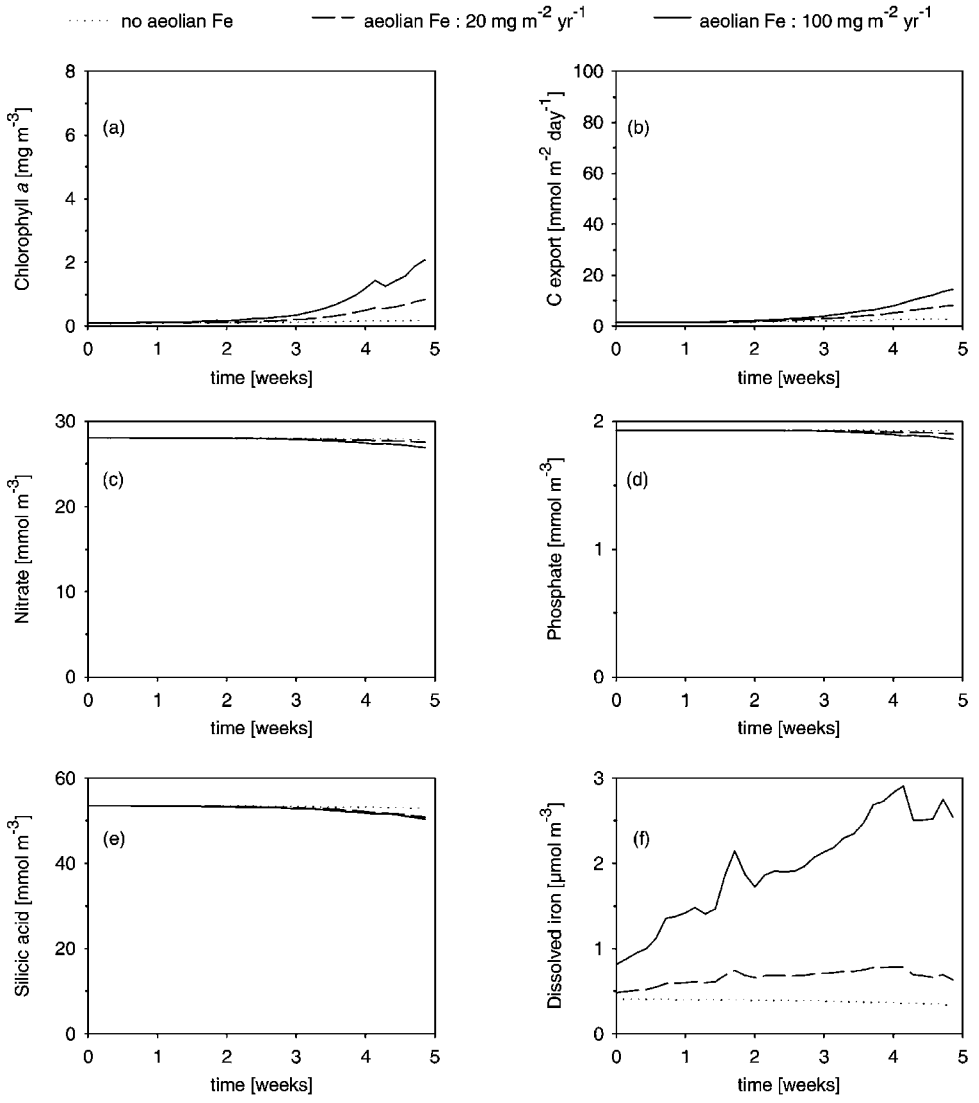

Fig. 8. SWAMCO model response of diatom-Chl *a* (a), carbon export production (b), nitrate (c), phosphate (d), silicic acid (e), and dissolved iron (f) to continuous atmospheric inputs of iron (0–100 mg m^{-2} yr^{-1}) in the marginal ice zone (MIZ) over the period of the ANT X/6 cruise.

enrichment above 0.5 µmol m^{-3} (Figs. 7 and 8). Below this concentration no phytoplankton accumulation is predicted (Fig. 8). Initial diatom abundance at the time of sufficient light and iron fertilization is important as well (Figs. 7 and 8) and determines the timing of the bloom. This indicates that the resulting effect of natural (de Baar et al., 1995) or intentional (SOIREE, Boyd et al., in preparation) iron enrichment will depend on both the meteorological conditions and the pre-existing diatom biomass.

Table 7
Sensitivity of the diatom production, *f* ratio (NO_3 upt./N_{tot} upt.), export production (carbon, opal, Si : C ratio) to continuous atmospheric iron inputs, tested by the SWAMCO model in the Polar Frontal region (PFr) and the Marginal Ice Zone (MIZ) during austral spring 1992. All constraints except iron are those met during ANTX/6 cruise

	Fe input (mg m^{-2} yr^{-1})	Diatom-C production (mol m^{-2})	*f* ratio —	Carbon export (mol m^{-2})	Opal export (mol m^{-2})	[Si : C] export (mol : mol)
PFr	0	1.34	0.80	0.82	0.44	0.54
	1	1.36	0.80	0.83	0.44	0.53
	20	1.64	0.82	0.90	0.48	0.53
	100	2.45	0.84	1.08	0.47	0.43
MIZ	0	0.071	0.80	0.070	0.022	0.31
	1	0.079	0.80	0.072	0.023	0.32
	20	0.22	0.81	0.113	0.053	0.47
	100	0.39	0.83	0.16	0.059	0.37

One major result of the SWAMCO scenarios is the simulated shift in nutrient limitation of diatoms, from iron to silicate limitation, under the scenario of maximum iron enrichment in the PFr (Figs. 7a, e and f). At the same time nitrates are never depleted (Fig. 7c). Combined with the predicted f_{NO_3} of 0.80 (Table 7) this indicates that such an imbalance between nitrate and silicate assimilation by diatoms results from the high silicification level of diatoms. From these scenarios, the maximum spring diatom biomass reached in the PFr can be evaluated at 7.5 mg Chl *a* m^{-3} (Fig. 7a). The corresponding maximum predictions for the spring diatom and export production are, respectively, 2.45 and 1.08 mmol C m^{-2} (Table 7). As a general trend the export production of particulate carbon is linearly related to diatom production for values of the latter which are higher than 0.1–0.2 mmol C m^{-2} (Table 7). Under such conditions and in the absence of mesozooplankton, the model calculates that 50% of diatom production is exported out of the surface layer (Table 7). On the other hand, opal export production does not increase significantly with iron enrichment (Table 7) due to the negative dependence of diatom silicification on ambient iron (Table 4). In other words, the computed Si : C ratios of export production are negatively related to available iron (Table 7).

4.2.2. Sensitivity of the SWAMCO prediction of diatom blooms to iron and silicon parameterization

Considering the key role of Fe and Si in regulating diatom blooms and opal export production, several SWAMCO runs were conducted at the Polar Frontal region to explore the model response to changing values of the parameters describing the diatom Fe and Si uptake. These are the half-saturation constant for Fe and Si uptake [K_{FeDIA} and K_{si}] and the cellular Fe and Si content [Fe : C and Si : C]. The ranges of tested values were those reported for diatoms by Sunda and Huntsman (1997) and

Table 8
SWAMCO model: Sensitivity test to iron and silicon physiology parametrization (cellular stoichiometry and 1/2 saturation constant of uptake). Diatom production, export production, in the upper 100 m, integrated over the period of the ANT X/6 cruise (austral spring 1992, Polar Frontal region)

	Diatom-C production (mol m^{-2})	BSi production (mol m^{-2})	C export (mol m^{-2})	Si export (mol m^{-2})	Si : C_{export} (mol : mol)
(a) *Iron*					
Fe : C (mol : mol)					
0.02	2.53		1.06	0.50	0.47
0.1	2.08		0.98	0.53	0.54
0.2[a]	**1.35**		**0.82**	**0.44**	**0.54**
K_{Fe} (μmol m^{-3})					
0.18	1.50		0.95	0.55	0.58
1.2[a]	**1.35**		**0.82**	**0.44**	**0.54**
1.8	1.26		0.75	0.38	0.50
(b) *Silicon*					
Si : C (mol : mol)					
0.13	1.35	0.065	0.82	0.08	0.10
0.6	1.35	0.38	0.82	0.26	0.31
1.4	1.35	0.92	0.82	0.55	0.67
1.52–0.39 [Fe][a]	**1.35**	**0.77**	**0.82**	**0.44**	**0.54**
K_{Si} (mmol m^{-3})					
4[a]	**1.35**	**0.77**	**0.82**	**0.44**	**0.54**
20	1.31	0.74	0.78	0.41	0.53
80	0.26	0.69	0.27	0.08	0.31

[a]Data in bold: reference simulation.

Brzezinski (1985) for Fe and by Conley et al. (1989) and Nelson and Tréguer (1992) for Si. Results of these scenarios are analyzed in terms of diatom production and carbon and opal export production (Table 8). The magnitude of the diatom bloom and the carbon export production are not much dependent on the half-saturation constant for Fe uptake in the range 0.18–1.8 μmol Fe m^{-3} (Table 8a). More sensitive is the dependence on the iron to carbon stoichiometry, which shows a + 22 and − 35% variation of the SWAMCO reference diatom production with tested values of Fe : C between 0.02 and 0.2 (Table 8a). Furthermore, model scenarios show that the exported fraction of carbon production is positively related to the cellular iron content (Table 8a). The variability of the computed Si : C ratio of export production (Table 8a) results from the dependence of the diatom silicification level on ambient iron. This is clearly evidenced by scenarios testing the variability of opal export production and Si : C ratios for different parameterization of the diatom Si stoichiometry between 0.13 and 1.4 (Table 8b). Opal export production simulated with the currently used Si : C of 0.13, chosen as typical of coastal diatoms (Brzezinski, 1985), is 5 times less than the flux calculated with the iron-dependent silicon stoichiometry. On the contrary, little dependence to K_{Si} of opal production and export production is predicted for values up to 20 mmol m^{-3}. Only the less probable K_{Si} value of 80 mmol m^{-3} shows a strong

limitation of diatom production (Table 8b). These results reveal the complex interplay of Si and Fe limitation in regulating diatom blooms and the associated biogeochemical cycles in the Southern Ocean, as already suggested by laboratory and field observations (Takeda, 1998; Hutchins and Bruland, 1998; de Baar et al., 1999). These SWAMCO scenarios strongly indicate that more investigations on the nutrient dynamics of phytoplankton are needed to understand mechanisms driving export production events in the Southern Ocean. They indicate as well that simple models based on a limitation of phytoplankton production by a single element are not suitable for investigation of the carbon cycle in the Southern Ocean.

5. Concluding remarks

Ever since Brandt (1899) the paradigm of a single limiting factor for phytoplankton blooms has repeatedly been invoked in plankton ecology. For the Southern Ocean singular limitation by either light, grazing losses or Fe limitation has now and then been advocated (Tranter, 1982; Martin and Fitzwater, 1988; Mitchell and Holm-Hansen, 1991; Dugdale and Wilkerson, 1990). The paradigm of a single controlling factor has been argued against (de Baar, 1994), as being an inappropriate extrapolation of the law of the minimum (Liebig von et al., 1840) beyond its validity for harvested crops, and having to give way to a realistic concept of ever-changing complex interactions of multiple growth and loss factors. The latter concept now appears confirmed by the complex interplay of rate and state variables in the SWAMCO model being required to be able to simulate the austral spring 1992 observations in the Antarctic Ocean.

Clearly, one is beginning to understand some first basic principles of plankton dynamics of the Southern Ocean, but more is to be learned. The generic design of the model appears robust but will have to be further verified with new observational data sets of similar extent and coherence as SO-JGOFS ANT X/6 but in other regions and seasons of the Southern Ocean, in particular to address the role of metazooplankton in food-web export. Also the model, while complicated, is modest when one reflects on the very intricate and diverse plankton community in real oceanic waters. For instance, the non-siliceous *Phaeocystis* colonies, which form massive blooms in the Ross Sea and Prydz Bay, have yet to be incorporated in the current model for further application at the scale of the global Southern Ocean. Ongoing research on the speciation of different chemical forms of Fe in seawater affecting uptake of Fe by the cell will provide the basis for further refinements in the model. Finally, several physical forcing functions known to exist have inadequate (e.g. meandering of Polar Front) or virtually non-existing (stabilizing mechanisms at Polar Front in 1992) observational data sets for validation, hence cannot yet be incorporated into the model.

Acknowledgements

This work was part of the Belgian research project BELCANTO funded under contract N° A4/DD/B12 in phase IV of the Belgian Research Program on Antarctic

and of the European Union CARUSO project funded under contract N°ENV4-CT97-0472 by the Environment and Climate Program of the European Commission. Most of the data used for the model implementation and validation were collected during three SO-JGOFS polar expeditions (ANTX/6 and ANTARES-2,3). We express our gratitude to Victor Smetacek, Uli Bathmann and Paul Tréguer, the colleagues responsible for the German and French SO-JGOFS Programs, who took an active part in the implementation and coordination of research activities. We are grateful to two anonymous referees for their critical and constructive comments that greatly improved the manuscript.

References

Arrigo, K.R., Weiss, A.M., Smith Jr, W.O., 1998a. Physical forcing of phytoplankton dynamics in the southwestern Ross Sea. Journal of Geophysical Research 103 (C1), 1007–1021.

Arrigo, K.R., Worthen, D., Schnell, A., Lizotte, M.P., 1998b. Primary production in Southern Ocean waters. Journal of Geophysical Research 103 (C8), 15587–15600.

de Baar, H.J.W., 1994. Von Liebig's law of the minimum and phytoplankton ecology (1899–1999). Progress in Oceanography 33, 347–386.

de Baar, H.J.W., Buma, A.G.J., Nolting, R.F., Jacques, G., Tréguer, P., Cadée, G.C., 1990. On iron limitation of the Southern Ocean: experimental observations in the Weddell and Scotia Seas. Marine Ecology Progress Series 65, 105–122.

de Baar, H.J.W., de Jong, J.T.M., Bakker, D.C.E., Veth, C., Bathmann, U.W., Löscher, B.M., 1995. Importance of iron for plankton blooms and carbon dioxide drawdown in the southern Ocean. Nature 373, 412–415.

de Baar, H.J.W., Van Leeuw, M.A., Siharek, R., Goeyens, L., Bakker, K.M.J., Fritsches, P., 1997. Deep Sea Research II 44 (1–2), 229–260.

de Baar, H.J.W., Boyd, P.W., 1999. The role of iron in plankton ecology and carbon dioxide transfer of the Global Oceans. In: Hanson, R.B., Ducklow, H.W., Filed, J.G. (Eds.), The Dynamic Ocean Carbon Cycle: A Midterm Synthesis of the Joint Global Ocean Flux Study. International Geosphere Biosphere Book Series, Cambridge University Press, Chapter 4, 61–141.

de Baar, H.J.W., de Jong, J.T.M., Nolting, R.F., Timmermans, K.R., van Leeuwe, M.A., Bathmann, U., Rutgers van der Loeff, M., Sildam, J., 1999. Low dissolved Fe and the absence of diatom blooms in remote Pacific waters of the Southern Ocean. Marine Chemistry 66, 1–34.

Bathmann, U.V., Scharek, R., Klaas, C., Smetacek, V., Dubischaar, C.D., 1997. Spring development of phytoplankton biomass and composition in major water masses of the Atlantic sector of the Southern Ocean. Deep-Sea Research II 44 (1–2), 51–68.

Becquevort, S., 1997. Nanoprotozooplankton in the Atlantic sector of the Southern Ocean during early spring: biomass and feeding activities. Deep-Sea Research II 44 (1–2), 355–373.

Becquevort, S., 1999. Importance du réseau trophique microbien dans l'Océan Anatrctique: rôle du protozooplankton. Ph.D. Dissertation, Université Libre de Bruxelles.

Bianchi, F., Boldrin, A., Cioce, F., Kuosa, H., Larsson, A.M., Dieckmann, G., 1993. Phytoplankton distribution in relation to sea ice, hydrography and nutrients in the northwestern Weddell Sea in early spring 1988 during EPOS. Polar Biology 12, 225–236.

Billen, G., 1990. Delayed development of bacterioplankton with respect to phytoplankton: a clue for understanding their trophic relationships. Archiv Hydrobiologishes Beiheft Ergebnisse Limnology 34, 94–98.

Billen, G., Becquevort, S., 1991. Phytoplankton-bacteria relationship in the Antarctic marine ecosystem. Polar Research 10, 245–263.

Billen, G., Servais, P., 1988. Modélisation des processus de dégradation bactérienne de la matière organique en milieu aquatique. In: Bianchi, M., et al. (Eds.), Micro-organismes dans les écosystèmes océaniques. Masson, Paris, pp. 219–245.

Björnsen, P.K., Kuparinen, J., 1991. Growth and herbivory by heterotrophic dinoflagellates in the Southern Ocean studied by microcosm experiments. Marine Biology 109, 397–405.

Boyd, P.W., Muggli, D.L., Varela, D.E., Chretien, R., Harrison, P.J., Goldblatt, R.H., 1996. In vitro iron enrichment experiments in the NE Subarctic Pacific. Marine Ecology Progress Series 136, 179–193.

Brand, L.E., 1991. Minimum iron requirements of marine phytoplankton and the implications for biogeochemical control of new production. Limnology and Oceanography 36 (8), 1756–1771.

Brandt, K., 1899. Veber den Stoffwechsel in Meer (Rektoratsrede). Wissenschaftliche Meeresundersuchungen, Abteilung Kiel, Neue Folge 4, 215–230.

Brzezinski, M.A., 1985. The Si : C : N ratio of marine diatoms: interspecific variability and the effect of some environmental variables. Journal of Phycology 2, 347–357.

Buma, A.G., de Baar, H.J.W., Nolting, R.F., van Bennekom, A.J., 1991. Metal enrichment experiments in the Weddell Sea: effects of Fe and Mn on various plankton communities. Limnology and Oceanography 36, 1865–1878.

Campbell, J.W., Aarup, T., 1989. Photosynthetically available radiation at high latitudes. Limnology and Oceanography 34, 1277–1290.

Cavenders-Bares, K.K., Mann, E.L., Chisholm, S.W., Ondrusek, M.E., Bidigare, R.R., 1999. Differential response of equatorial Pacific phytoplankton to iron fertilization. Limnology and Oceanography 44, 237–246.

Chase, Z., Price, N.M., 1997. Metabolic consequences of iron deficiency in heterotrophic marine protozoa. Limnology and Oceanography 42, 1673–1684.

Chavez, F.P., Buck, K.R., Coale, K.H., DiTullio, N.A., Welschmeyer, G.R., Jacobson, A.C., Barber, R.T., Martin, R.T.J.H., 1991. Growth rates, grazing, sinking, and iron limitation of equatorial Pacific phytoplankton. Limnology and Oceanography 36, 1816–1833.

Coale, K.H., Fitzwater, S.E., Gordon, R.M., Barber, R.T., Johnson, K.S., 1996. Control of community growth and export production by upwelled iron in the equatorial Pacific Ocean. Nature 379, 621–624.

Cohen, D., Parnas, H., 1976. An optimal policy for the metabolism of storage materials in unicellular algae. Journal of Theoretical Biology 56, 1–18.

Conley, D.J., Kilham, S.S., Theriot, E., 1989. Differences in silica content between marine and freshwater diatoms. Limnology and Oceanography 34, 205–212.

Cuhel, R.L., Ortner, P.B., Lean, D.R.S., 1984. Night synthesis of protein by algae. Limnology and Oceanography 29, 731–744.

Dehairs, F., Shopova, D., Ober, S., Veth, C., Goeyens, L., 1997. Particulate barium stocks and oxygen consumption in the Southern Ocean mesopelagic water column during spring and early summer: relationship with export production. Deep Sea Research II 44 (1–2), 497–516.

Denman, K.L., 1973. A time-dependent model of the upper ocean. Journal of Physical Oceanography 3, 173–184.

Dubischar, C.D., Bathmann, U.V., 1997. Grazing impact of copepods and salps on phytoplankton in the Atlantic sector of the Southern Ocean. Deep-Sea Research II 44 (1–2), 415–434.

Dugdale, R.C., Wilkerson, F.P., 1990. Iron addition experiments in the Antarctic: a re-analysis. Global Biogeochemical Cycles 4, 13–19.

El-Sayed, S.Z., 1984. Productivity of the Antarctic waters: a reappraisal. In: Holm-Hansen, O., Bolis, L., Gilles, R. (Eds.), Marine Phytoplankton and Productivity. Springer, Berlin, pp. 19–34.

Elskens, M., Goeyens, L., Dehairs, F., Joint, A., Baeyens, W., Rees, J., 1997. Improved estimation of f-ratio in naturalphytoplankton assemblages. In: Dehairs, F., Elskens, M., Goeyens, L. (Eds.), Integrated Marine System Analysis. Vrij Universiteit Brussel Press, pp. 139–152.

Fileman, T.W., Pond, D.W., Barlow, R.G., Mantoura, R.F.C., 1998. Vertical profiles of pigments, fatty acids and amino acids: Evidence for undegraded diatomaceous material sedimenting to the deep ocean in the Bellingshausen Sea. Antarctica. Deep-Sea Research 45, 333–346.

Fitzwater, S.E., Coale, K.H., Gordon, R.M., Ondrusek, M.E., Johnson, K.S., 1996. Iron deficiency and phytoplankton growth in the equatorial Pacific. Deep-Sea Research II 43, 995–1015.

Fransz, H.G., Gonzales, S.R., 1997. Latitudinal metazoan plankton zones in the Antarctic Circumpolar Current along 6°W during Austral spring 1992. Deep-Sea Research II 44 (1–2), 395–414.

Frost, B.W., Franzen, N.C., 1992. Grazing and iron limitation in the control of phytoplankton stock and nutrient concentration: a chemostat analogue of the Pacific equatorial upwelling zone. Marine Ecology Progress Series 83, 291–303.

Gerringa, L.J.A., de Baar, H.J.W., Timmermans, K.R., 2000. Iron limitation of phytoplankton growth in natural waters versus artificial laboratory media with EDTA. Marine Chemistry 68, 335–346.

Goeyens, L., Tréguer., Lancelot, C., Mathot, S., Becquevort, S., Morvan, J., Dehairs, F., Baeyens, W., 1992. Ammonium regeneration in the Scotia Weddell Confluence area during spring 1988. Marine Progress Series 78, 241–252.

Goosse, H., Hecq, J.-H., 1994. Modelling the ice–ocean–plankton interactions in the Southern Ocean. Journal of Marine Systems 5, 471–484.

Gordon, A.L., Molinelli, J., Baker, T.N., 1986. Southern Ocean Atlas. Columbia University Press, New York.

Gran, H.H., 1931. On the conditions for the production of plankton in the sea. Rapport du Conseil International pour l' Exploration de la Mer 75, 37–46.

Harrison, W.G., Harris, L.R., Irwin, B.D., 1996. The kinetics of nitrogen utilization in the oceanic mixed layer: nitrate and ammonium interactions at nanomolar concentrations. Limnology and Oceanography 41, 16–32.

Harvey, H.W., 1933. On the rate of diatom growth. Journal of Marine Biology Association UK 19, 253–276.

Harvey, H.W., 1937. The supply of iron to diatoms. Journal of Marine Biology Association UK 22, 205–219.

Helbling, E.W., Villafane, V., Holm-Hansen, O., 1991. Effect of iron on productivity and size distribution of Antarctic phytoplankton. Limnology and Oceanography 36, 1879–1885.

Hewes, C.D., Sakshaug, E., Reid, F.M., Holm-Hansen, O., 1990. Microbial autotrophic and heterotrophic eucaryotes in Antarctic waters: relationships between biomass and chlorophyll aolenosine triphosphate and particulate organic carbon. Marine Ecology Progress Series 63, 27–35.

Holm-Hansen, O., Mitchell, B.G., 1991. Spatial and temporal distribution of phytoplankton and primary production in the western Bransfield Strait region. Deep-Sea Research II 38, 961–980.

Hoppema, M., Goeyens, L., 1999. Redfield behavior of carbon, nitrogen and phosphorus depletion in Antarctic surface water. Limnology and Oceanography 44 (1–2), 220–224.

Hutchins, D.A., 1995. Iron and the marine community. In: Chapmann, D., Round, E. (Eds.), Progress in Phycological Research, Vol. 11. Biopress, Bristol, pp. 1–49.

Hutchins, D.A., Wang, W., Fisher, N.S., 1995. Copepod grazing and the biogeochemical fate of diatom iron. Limnology and Oceanography 40, 989–994.

Hutchins, D.A., Bruland, K.W., 1998. Iron-limited diatom growth and Si:N uptake ratios in a coastal upwelling regime. Nature 393, 561–564.

Hutchins, D.A., Witter, A.M., Butler, A., Luther, G.W., 1999. Competition among marine phytoplankton for different chelated iron species. Nature 400, 858–861.

Jackson, G.A., 1990. A model of the formation of marine algal flocs by physical aggregation processes. Deep-Sea Research 37, 1197–1211.

Jochem, F.J., Mathot, S., Quéguiner, B., 1995. Size-fractionated primary production in the open Southern Ocean in austral spring. Polar Biology 15, 381–392.

Kristiansen, S., Syvertsen, E.E., Farbrot, T., 1992. Nitrogen uptake in the Weddell Sea during late winter and spring. Polar Biology 12, 245–252.

Lancelot, C., Mathot, S., Owens, N.J.P., 1986. Modelling protein synthesis, a step to an accurate estimate of net primary production: The case of Phaeocystis pouchetii colonies in Belgian coastal waters. Marine Ecology Progress Series 32, 193–202.

Lancelot, C., Veth, C., Mathot, S., 1991a. Modelling ice-edge phytoplankton bloom in the Scotia-Weddell Sea sector of the Southern Ocean during spring 1988. Journal of Marine Systems 2, 333–346.

Lancelot, C., Billen, G., Veth, C., Mathot, S., Becquevort, S., 1991b. Modelling carbon cycling through phytoplankton and microbes in the Scotia-Weddell Sea area during sea ice retreat. Marine Chemistry 35, 305–324.

Lancelot, C., Mathot, S., Veth, C., de Baar, H.W.J., 1993. Factors controlling phytoplankton ice-edge blooms in the marginal ice-zone of the north western Weddell Sea during sea ice retreat 1988: field observations and mathematical modelling. Polar Biology 13, 377–387.

Lancelot, C., Becquevort, S., Menon, P., Dandois,. J.M., Mathot, S., 1997. In: Caschetto, S. (Ed.), Ecological Modelling of the Planktonic Microbial Food-Web. Belgian Research Programme on the Antarctic, Scientific Results of Phase III 1992–1996, 1, pp. 1–78.

van Leeuwe, M.A., Scharek, R., de Baar, H.J.W., Goeyens, L., de Jong, J.T.M., 1997. Iron enrichment experiments in the Southern Ocean: physiological responses of plankton communities. Deep-Sea Research II 44 (1–2), 189–208.

Leonard, C.L., Mc Clain, C.R., Murtugudde, R., Hofmann, E.E., Harding Jr, L.W., 1999. An iron-based ecosystem model of the central equatorial Pacific. Journal of Geophysical Research 104, 1325–1341.

Liebig von, J., 1840. Organic chemistry and its application to agriculture and physiology. Taylor and Walton, London.

Lochte, K., Bjorsen, P.K. Giesenhagen, H., Weber, A., 1997. Bacterial standing stock and production and their relation to phytoplankton in the Southern Ocean. Deep-Sea Research II 44 (1–2), 321–340.

Löscher, B.M., de Baar, H.J.W., de Jong, J.T.M., Dehairs, F., Veth, C., 1997. The distribution of iron in the Antarctic Circumpolar Current. Deep-Sea Research II 44 (1–2), 143–188.

Martin, J.H., Fitzwater, S.E., 1988. Iron deficiency limits phytoplankton growth in the North-East Pacific Subarctic. Nature 331, 341–343.

Martin, J.H., Gordon, R.M., Fitzwater, S.E., 1990. Iron in Antarctic waters. Nature 345, 156–158.

Mathot, S., 1995. Phytoplankton in the marginal ice zone and its contribution to the annual primary production of the Southern Ocean. Ph. D. Dissertation, Université Libre de Bruxelles.

Mathot, S., Lancelot, C., Dandois, J.-M., 1992. Gross and net primary production in the Scotia-Weddell Sea sector of the Southern Ocean during spring 1988. Polar Biology 12, 321–332.

Mitchell, B.G., Holm-Hansen, O., 1991. Observations and modelling of the phytoplankton crop in relationship to mixing depth. Deep-Sea Research II 38, 981–1008.

Morel, F.M.M., Rueter, J.G., Price, N.M., 1990. Iron nutrition of phytoplankton and its possible importance in the ecology of ocean regions with high nutrient and low biomass. Oceanography 4 (2), 56–61.

Muggli, D.L., Lecourt, M., Harrison, P.J., 1996. Effects of iron and nitrogen source on the sinking rate, physiology and metal composition of an oceanic diatom from the subarctic Pacific. Marine Ecology Progress Series 132, 215–227.

Nelson, D.M., Smith, W.O., Gordon, L.I., Huber, B.A., 1987. Spring distribution of density, nutrients and phytoplankton biomass in the ice-edge zone of the Weddell-Scotia Sea. Journal of Geophysical Research 92 (C7), 7181–7190.

Nelson, D.M., Tréguer, P., 1992. Role of silicon as limiting nutrient to Antarctic diatoms: evidence from kinetics studies in the Ross Sea ice-edge zone. Marine Ecology Progress Serics 80, 255–264.

Nolting, R.F., Gerringa, L., Swagerman, R., Timmermans, K.R., de Baar, H.J.W., 1998. Fe(III) speciation in the High Nutrient Low Chlorophyll Pacific region of the Southern Ocean. Marine Chemistry 62, 335–352.

Platt, T.C., Gallegos, L., Harrisson, W.G., 1980. Photoinhibition of photosynthesis in natural assemblages of marine phytoplankton. Journal of Marine Research 38, 687–701.

Pondaven, P., Fravolo, C., Ruiz-Pino, D., Tréguer, P., Quéguiner, B., Jeandel, C., 1998. Modeling the silica pump in the permanently open ocean zone of the Southern Ocean. Journal of Marine Systems 17, 587–619.

Price, N.M., Ahner, B.A., Morel, F.M.M., 1994. The equatorial Pacific ocean: grazer-controlled phytoplankton population in an iron-limited ecosystem. Limnology and Oceanography 39, 520–534.

Quéguiner, B., Tréguer, P., Peeken, I., Scharek, R., 1997. Biogeochemical dynamics and the silicon cycle in the Atlantic sector of the Southern Ocean during austral spring 1992. Deep-Sea Research II 44, 69–90.

Redfield, A.C., Ketchum, B.H., Richards, F.A., 1963. The influence of organisms on the composition of seawater In: Hill, M.N. (Ed.), The Sea (2). Interscience, New York, pp. 26–77.

Rommets, J.W., Stoll, M.H.C., de Koster, R.X., de Baar, H.J.W., Bathmann, U.V., de Bruin, T.F., 1997. The CD-ROM Database of the JGOFS expedition ANTX/6 aboard R.V. Polarstern. Deep-Sea Research II 44, 517–519.

Rutgers van der Loeff, M.M., Friedrich, J., Bathmann, U.V., 1997. Carbon export during the spring bloom at the Antarctic Polar Front, determined with the natural tracer 234th. Deep-Sea Research II 44, 457–478.

Scharek, R., van Leeuwe, M.A., de Baar, H.J.W., 1997. Responses of Southern Ocean phytoplankton to the addition of trace metals. Deep-Sea Research II 44, 209–228.

Servais, P., Billen, G., Hascoët, M., 1987. determination of the biodegradable fraction of dissolved organic matter in waters. Water Research 21, 445–450.

Shuter, B., 1979. A model of physiological adaptation in unicellular algae. Journal of Theoretical Biology 78, 519–552.

Smetaeck, V., Scharek, R., Nötig, E.-M., 1990. Seasonal and regional variation in the pelagial and its relationship to the life history. In: Kerry, K.R., Hempel, G. (Eds.), Antarctic Ecosystems: Ecological Change and Conservation. Springer, Berlin, pp. 103–114.

Smetacek, V., de Baar, H.J.W., Bathmann, U.V., Rutgers van der Loeff, M.M., Lochte, K., 1997a. Ecology and biogeochemistry of the Antarctic Circumpolar Current during austral spring: a summary of Southern Ocean JGOFS cruise ANTX/6 of R. V. Polarstern. Deep-Sea Research II 44 (1–2), 1–22.

Smetacek, V., de Baar, H.J.W., Bathmann, U.V., Rutgers van der Loeff, M.M., Lochte, K., 1997b. Ecology and biogeochemistry of the Antarctic Circumpolar Current during Austral spring: Southern Ocean JGOFS cruise ANTX/6 of R.V. Polarstern. Deep-Sea Research II 44(1–2), 519pp.

Smith, W.O., Nelson, D.M., 1985. Phytoplankton bloom produced by a receeding ice edge in the Ross Sea: spatial coherence with the density field. Science 227, 163–166.

Smith Jr, W.O., Nelson, D.M., 1986. The importance of ice-edge phytoplankton blooms in the Southern Ocean. Bioscience 36, 251–257.

Somville, M., Billen, G., 1983. A method for determination exoproteolytic activity in natural waters. Limnology and Oceanography 28, 190–193.

Sullivan, C.W.C., Mc Clain, R., Comiso, J.C., Smith, W.O., 1988. Phytoplankton standing crops within an Antarctic Ice Edge assessed by Satellite Remote Sensing. Journal of Geophysical Research 93 (C10), 12487–12498.

Sunda, W.G., Huntsman, S.A., 1995. Iron uptake and growth limitation in oceanic and coastal phytoplankton. Marine Chemistry 50, 189–206.

Sunda, W.G., Huntsman, S.A., 1997. Interrelated influence of iron, light and cell size on marine phytoplankton growth. Nature 390, 389–392.

Sunda, W.G., Swift, D., Huntsman, S.A., 1991. Iron growth requirements in oceanic and coastal phytoplankton. Nature 351, 55–57.

Takeda, S., 1998. Influence of iron availability on nutrient consumption ratio of diatoms in oceanic waters. Nature 393, 774–777.

Tortell, P.D., Maldonado, M.T., Price, N.D., 1996. The role of heterotrophic bacteria in iron-limited ocean ecosystems. Nature 383, 330–332.

Tranter, D.J., 1982. Interlinking of physical and biological processes in the Antarctic Ocean. Oceanography and Marine Biology, Annual Review 20, 11–35.

Turner, D.R., Owens, N.P.J., 1995. A biogeochemical study in the Bellinghausen Sea: overview of the STERNA 1992 expedition. Deep-Sea Research II 42 (4–5), 907–933.

Veth, C., 1991a. The evolution of the upper water layer in the marginal ice zone, austral spring 1988. Scotia-Weddell Sea. Journal of Marine Systems 2, 451–464.

Veth, C., 1991b. The structure and evolution of the top layer of the water column accross the marginal ice zone during spring 1988 in the Scotia-Weddell Sea sector of the Southern Ocean. Marine Chemistry 35, 63–76.

Veth, C., Lancelot, C., Ober, S., 1992. On processes determining the vertical stability of surface waters in the marginal ice zone of the Northwestern Weddell Sea and their relationship with phytoplankton bloom development. Polar Biology 12, 237–243.

Veth, C., Peeken, I., Scharek, R., 1997. Physical anatomy of fronts and surface waters in the ACC near the 6°W meridian during austral spring 1992. Deep-Sea Research II 44 (1–2), 23–50.

Zettler, G.R., Olson, R.J., Binder, B.J., Fitzwater, S.W., Gordon, R.M., Chisholm, S.E., 1996. Iron-enrichment bottle experiments in the equatorial Pacific: response of individual cells. Deep-Sea Research II 43, 1017–1029.